INTERNATIONAL ATOMIC ENERGY AGENCY
UNITED NATIONS EDUCATIONAL, SCIENTIFIC AND CULTURAL ORGANIZATION

INTERNATIONAL CENTRE FOR THEORETICAL PHYSICS
34100 TRIESTE (ITALY) - P.O.B. 586 - MIRAMARE - STRADA COSTIERA 11 - TELEPHONES: 224281/2/3/4/5/6
CABLE: CENTRATOM - TELEX 460392-1

SMR/94- 55

SPRING COLLEGE ON AMORPHOUS SOLIDS
AND THE LIQUID STATE

14 April - 18 June 1982

PROPERTIES OF TWO-LEVEL SYSTEMS

W.A. PHILLIPS

Cavendish Laboratory
Department of Physics
University of Cambridge
Madingley Road
Cambridge CB3 0HE
UK

1. GENERAL INTRODUCTION

1.1 Heat Capacity and Thermal Conductivity

The easiest way to introduce this subject is by showing some early results on the thermal properties of vitreous silica and other amorphous solids. The heat capacity C and the thermal conductivity κ are shown as functions of the absolute temperature T in Figs 1.1 and 1.2. Also shown in these figures are C and κ for a similar crystalline material, α-quartz, which can be used to review the behaviour expected on the basis of simple theories.

The heat capacity of α-quartz varies as T^3 below 10 K, as expected on the Debye theory which predicts that in the long wavelength limit the density of phonon states $g(\omega)$ varies quadratically with the phonon frequency ω; $g(\omega) = A\omega^2$ if the velocity of sound v_s is a constant where $\omega q = v_s$, with q the phonon wavevector. At higher temperatures C increases more rapidly than T^3 as a result of the phonon dispersion which increases $g(\omega)$.

The temperature variation of the thermal conductivity, $\kappa \propto T^3$ can be most easily explained by means of the simple kinetic formula

$$\kappa = \frac{1}{3} C v_s \lambda \qquad 1.1$$

where λ is the phonon mean free path. At low temperatures phonons are scattered by defects in the crystal, or by the surfaces of the sample so that λ is independent of T. κ is therefore proportional to C and so to T^3. Above 40 K the reduction in λ by phonon-phonon scattering leads to the fall in κ.

These ideas are well known, and serve to emphasize the peculiarity of the results in the glass. C varies roughly as T below 1 K, and at 0.1 K is about two orders of magnitude greater in the glass than in the crystal. Below 1 K κ varies as T^2, in the range 4 to 30 K increases only slightly with T, and then increases at higher temperatures towards a value similar to that of quartz.

These results were soon supplemented by measurements on a wide range of other amorphous solids; oxide glasses, chalcogenide glasses, polymers and amorphous metals. In all these materials similar behaviour was observed, as can be seen for a representative sample in Figs 1.3 and 1.4.

1.2 Early Theories

The universality of the phenomena and the simplicity of the (idealized) temperature dependences C proportional to T and κ proportional to T^2 proved great attractions for theorists. A large number of different theories were

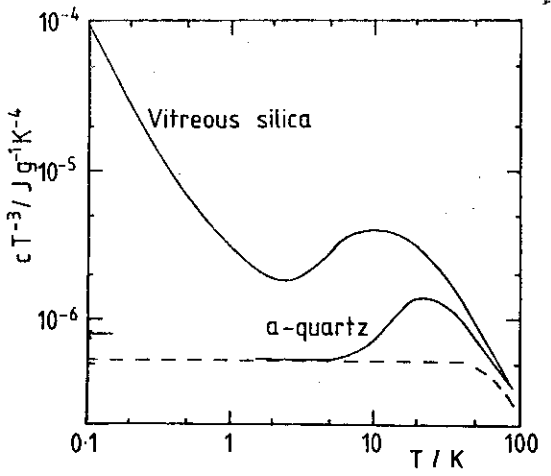

1.1 Heat capacity c of vitreous silica and crystalline quartz as a function of temperature T. (D.P. Jones Thesis, 1982, after R.C. Zeller and R.O. Pohl, Phys. Rev., B4, 2029, 1971.)

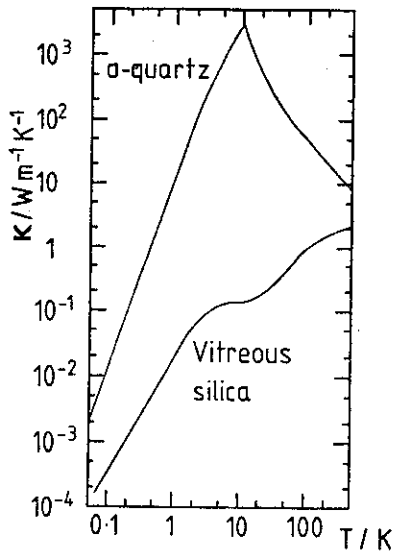

1.2 Thermal conductivity κ of vitreous silica and crystalline quartz. (D.P. Jones Thesis, 1982, after R.C. Zeller and R.O. Pohl, Phys. Rev., B4, 2029, 1971.)

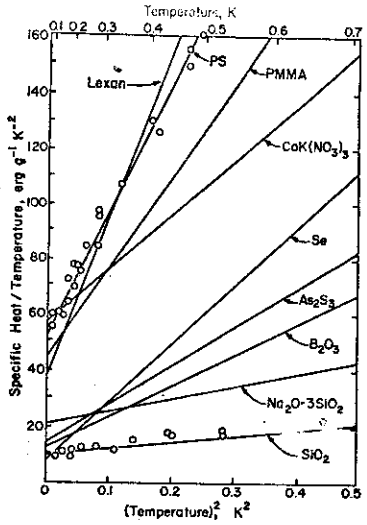

1.3 Heat capacity as a function of temperature for a range of glasses (R.B. Stephens, Phys. Rev., B8, 2896, 1973).

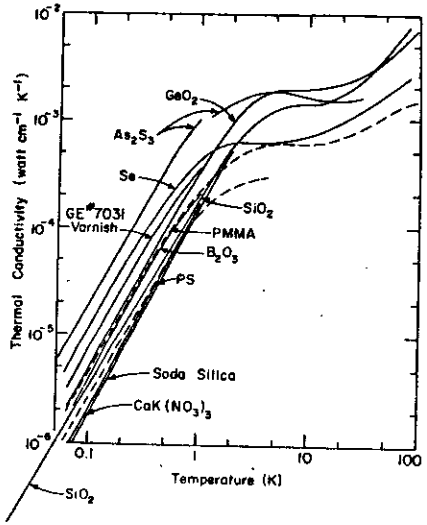

1.4 Thermal conductivity as a function of temperature for a range of glasses (R.B. Stephens, Phys. Rev., B8, 2896, 1973).

proposed in a short space of time. Some of these were based on realistic descriptions of the amorphous state, and are worth describing briefly in order to show how ideas from other branches of the study of amorphous solids can be applied to this field.

The first and perhaps most obvious explanation was in terms of electron states. In the amorphous state the sharp distinction between energy bands and energy gaps is blurred, and it was suggested that the specific heat was a result of the almost constant density of localised electron states at the Fermi level, giving a linear temperature dependent heat capacity just as electrons do in a metal. However, it turns out that the density of these localised states is much too small to explain the heat capacity. In silica for example the density of states deduced from the heat capacity is approximately $10^{46} J^{-1} m^{-3}$ (10^{21} ev^{-1} cm^{-3}) whereas optical measurements imply a density of states less than 10^{43} J^{-1} m^{-3}. After all, vitreous silica is almost perfectly transparent as can be shown by its use in optical fibres.

A second explanation involved the damping or scattering of phonons in a glass. This is based on the well-established idea that the lack of translational symmetry prevents the use of a wavevector q to describe the vibrational modes except at low frequencies where a continuum description should hold. A mode of well defined q will therefore decay as it propagates in the glass. Fulde and Wagner suggested a specific mechanism for this decay, based on structural relaxation, and suggested that this could explain not only the thermal conductivity but also (through the consequent broadening of the spectral response function) the heat capacity. However subsequent experiments, which will be described later, did not provide evidence for their mechanism, although the explanation of the thermal conductivity resembles current ideas.

The third and final example is a model for the thermal conductivity which is based on the scattering of sound waves by inhomogeneities in the glass structure. This is Rayleigh scattering by the local variations in the velocity of sound. However, two problems arise with this explanation. The first concerns the frequency or q dependence of the effect, as ω^4, ω^2 and ω dependences of the scattering rate have been suggested, and the second the magnitude of the fluctuations. Density fluctuations estimated thermodynamically or from light scattering experiments are too small, but there is no way of estimating the local variations of sound velocity. Such scattering is undoubtedly important above 1 K, but probably not at lower temperatures.

Many other theories have been suggested, but in most cases these theories are inconsistent with what is known of the amorphous state and with the more precise experiments which will now be described.

1.3 Acoustic Experiments

At 1 K the frequency of a thermal phonon, given by $\hbar\omega \sim kT$, is about 30 GHz. The properties of such phonons can be investigated directly by means of thermal Brillouin scattering. An incident photon excites or absorbs a phonon: measurements of the frequency shift at a particular scattering angle give the frequency and wavevector of the phonon, and the width of the Brillouin line gives the inverse phonon lifetime. Measurements show that both transverse and longitudinal acoustic phonons exist in a glass, and that there is no dispersion at these frequencies (i.e. the sound velocity is identical in SiO_2 with that measured at lower frequencies). The mean free path of these acoustic phonons is at least ten wavelengths at room temperature, and becomes larger as the temperature is reduced. Taken together with the thermal measurements these results show that additional excitations are present at low energies which contribute directly to the heat capacity and which scatter the existing phonons.

Acoustic measurements at lower frequencies, 100 MHz to 1 GHz, have provided a large amount of detailed information on the nature of these excitations. Many of these will be described later, but the results shown in Fig. 1.5 are particularly important. Below 1 K the attenuation increases with decreasing temperature if the acoustic intensity is low, just as expected on the basis of the thermal conductivity. The values of the phonon free path deduced from the acoustic measurements are consistent with those calculated from the thermal conductivity. However the most valuable aspect of these results from the point of view of investigating the low frequency excitations is the observed saturation of the attenuation at high acoustic intensities. The implication of these experiments is that the excitations must be represented by two-level systems and not for example by harmonic oscillators. This point will be considered later in more detail.

1.4 Tunnelling States

A specific form of the two-level system is provided by a tunnelling state. Indeed this model was suggested before the discovery of saturation and predicted the effect. The basic idea is that in contrast to a crystalline solid where the position of each atom is determined by symmetry, the amorphous solid contains atoms or groups of atoms which are equally happy to sit in either of two local potential minima. Indeed, it has been claimed

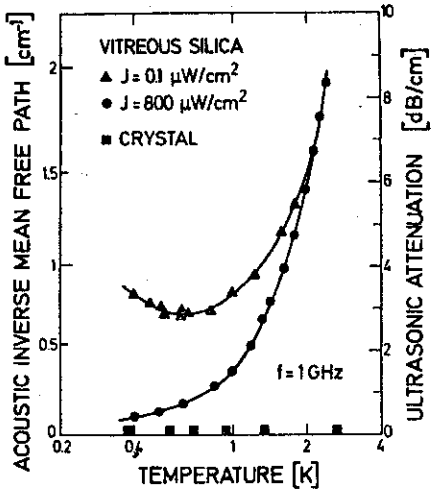

1.5 The ultrasonic attenuation as a function of temperature at high and low powers (S. Hunklinger and M. v Schickfus in Amorphous Solids: Low Temperature Properties, ed. W.A. Phillips, Springer, 1981 (Ref 1)).

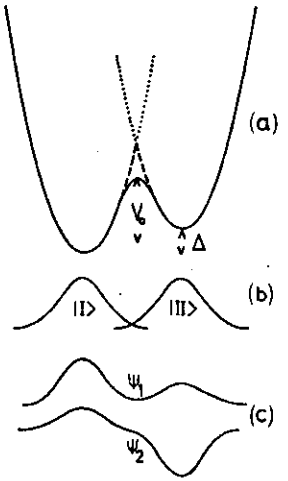

1.6 The double-well potential, together with the wavefunctions in the localised and diagonal representations.

that this is an essential property of the glass, representing the additional entropy frozen in at the glass transition T_g. If the barrier is not too large the atom can tunnel from one minimum to the other (just as in the ammonia molecule).

The state can be represented as in Fig. 1.6, and the quantum mechanical treatment of this double-well potential will now be considered in some detail.

The calculation of the energy levels of a particle in a double-well potential V of the form shown in Fig. 1.6a usually starts with the solution of the single-well problem shown in Fig. 1.6b. The choice of these two basis states is known as the *well, non-diagonal* or *localised* representation. Each state is the ground state of the appropriate harmonic potential V_1 or V_2, both of which are shown continued as dotted lines in Fig. 1.6a. The Hamiltonian can be written as

$$H = H_1 + (V - V_1) = H_2 + (V - V_2) \qquad 1.2$$

where H_1 and H_2 are the individual Hamiltonian operators. In this representation the Hamiltonian matrix becomes

$$\begin{pmatrix} E_1 + \langle 1|V - V_1|1\rangle & \langle 1|H|1\rangle \\ \langle 2|H|1\rangle & E_2 + \langle 2|V - V_2|2\rangle \end{pmatrix} \qquad 1.3$$

To a good approximation each term $\langle i|V - V_i|i\rangle$ can be neglected in comparison with E_i. If the zero of energy is chosen as the mean of the two ground state energies E_1 and E_2 eq. 1.3 can be written

$$\tfrac{1}{2}\begin{pmatrix} -\Delta & -\Delta_0 \\ -\Delta_0 & \Delta \end{pmatrix} \qquad 1.4$$

where Δ_0 is defined as

$$\Delta_0 = -2\langle 1|H|2\rangle \ , \qquad 1.5$$

the negative sign being introduced because the matrix element $\langle 1|H|2\rangle$ is negative. Notice that only if the wells are identical, apart from a relative displacement in energy, is the Δ of eq. 1.4 identical to that of Fig. 1.6a.

Δ_0 can be evaluated for specific potentials. For two identical three-dimensional harmonic oscillators with $\Delta = 0$ and with an overall potential shown by the dashed continuation in Fig. 1.6a

$$\Delta_0 = \hbar\omega_0\left[3 - \left(\frac{8V_o}{\pi\hbar\omega_0}\right)^{\frac{1}{2}}\right]e^{-2V_o/\hbar\omega_0} \qquad 1.6$$

where V_o is the minimum energy barrier between the two wells, and $\hbar\omega_0$ is equal to $2E_1$ or $2E_2$. Since for our purposes (and indeed for the localised representation to be useful) $V_o >> \hbar\omega_0$, eq. 1.6 becomes

$$\Delta_0 = -2\hbar\omega_0\left(\frac{2V_o}{\pi\hbar\omega_0}\right)^{\frac{1}{2}} e^{-2V_o/\hbar\omega_0}$$

$$= -4\left(\frac{2V_o^3\hbar^2}{md^2}\right)^{\frac{1}{4}} e^{-(2mV_o/\hbar^2)^{\frac{1}{2}}d/2} \qquad 1.7$$

where m is the mass of the particle and d the separation of the two minima. This value of Δ_0 is just twice that found for the equivalent problem in one dimension.

As an alternative example, the solution of Mathieu's equation for a rigid rotator in a twofold symmetric potential gives, in the same limit $V_o >> \hbar\omega_0$, the approximate result

$$\Delta_0 \simeq -8\hbar\omega_0\left(\frac{2V_o}{\pi\hbar\omega_0}\right)^{\frac{1}{2}} e^{-4V_o/\hbar\omega_0} \qquad 1.8$$

where again V_o is the height of the barrier separating the two wells, and ω_0 is the angular frequency of small oscillations with a single minimum.

Although both results imply a similar exponential dependence of Δ_0 on V_o the numerical relationships are different, and the use of a particular form of equation for Δ_0 cannot be justified unless, as is often the case in crystals, the microscopic symmetry of the potential is known. For this reason an expression of the form

$$\Delta_0 = -\hbar\Omega e^{-d(2mV_o/\hbar^2)^{\frac{1}{2}}} \qquad 1.9$$

where $\hbar\Omega$ is an energy roughly equal to $\hbar\omega_0$, is usually adequate in the case of amorphous solids. It is worth noting that $\langle 1|H|2\rangle$ is negative in these examples because the negative contribution from $V-V_2$ (for example) in eq. 1.2 overwhelms the positive contribution from H_2.

The matrix eq. 1.4 can be diagonalized to obtain the eigenstates, the *true, diagonal* or *energy* representation. The eigenfunctions, shown in Fig. 1.7c, have energies $\pm E/2$ where

$$E^2 = (\Delta^2 + \Delta_0^2) \qquad 1.10$$

and are usually written in the analytic forms

$$\psi_1 = |1\rangle\cos\theta + |2\rangle\sin\theta \qquad 1.11$$

$$\psi_2 = |1\rangle\sin\theta - |2\rangle\cos\theta \qquad 1.12$$

where $\tan 2\theta = \Delta_0/\Delta$. ψ_2 is the lower energy state because Δ_0 (as defined here) is positive.

The functions ψ_1 and ψ_2 defined by eqs 1.10 and 1.11 are orthonormal only to the extent that the overlap term $\langle 1|2\rangle$ can be put equal to zero. As far as normalization is concerned this presents no difficulty, as an additional multiplicative factor can be readily calculated, but may lead to more important problems in the calculation of matrix elements. Any matrix element involving the overlap of $\langle 1|$ and $|2\rangle$ must be evaluated carefully through a correct choice of orthonormal states.

It is worth pointing out the existence of a wide range of notation for 1.10. Not only have several symbols been used for the various energies in this equation but the same symbols have been used for half the energies. Occasional discrepancies of powers of two in formulae cited in the literature can often be traced to this difference in definition.

For this, as for any problem involving two energy levels, there is a formal analogy with the problem of a spin 1/2 particle in a magnetic field. The Hamiltonian matrix eq. 1.4 can be rewritten in terms of spin operators, although here too there is a choice of notation between the Pauli spin matrices

$$\sigma_x = \begin{pmatrix} 0 & 1 \\ 1 & 0 \end{pmatrix} \quad \sigma_y = \begin{pmatrix} 0 & -i \\ i & 0 \end{pmatrix} \quad \sigma_z = \begin{pmatrix} 1 & 0 \\ 0 & -1 \end{pmatrix} \qquad 1.13$$

and the spin -1/2 operators defined by $S_i = \frac{1}{2}\sigma_i$. After diagonalization the Hamiltonian can be written in the obvious form

$$H = \frac{1}{2} E\sigma_z \qquad 1.14$$

The advantages of this analogy will be seen later when it is used to interpret non-linear and coherent effects in the interaction of tunnelling states with acoustic and electric fields.

In many cases the results of experiments can be interpreted in terms of a simpler model which ignores the detailed origin of the two levels, and uses the energy E as the only parameter, in contrast to the tunnelling model which uses both Δ and Δ_0. This model is often known as the <u>two-level-system</u> model, in contrast to the <u>tunnelling</u> model described earlier.

The second step in the discussion of tunnelling states in amorphous solids involves an evaluation of the distribution functions for the parameters Δ_0 and Δ, the obvious choice of independent variables. Both parameters are expected to take a wide range of values in the amorphous solid. In the case of the asymmetry Δ it can be argued that the distribution function must be symmetric as positive and negative values of Δ are equally likely, and further

that the scale of energy variations will be determined by the thermal energy available at the effective temperature characterising the 'frozen liquid' state. Since T_g is between 300 and 1000 K for most glasses, this will be of the order of 0.05 eV. Below 1 K the thermal energy is 10^{-4} eV or less, so that the low temperature properties are sensitive to the centre of a broad symmetric distribution. The distribution function $f(\Delta)$ can therefore be taken to be a constant.

A less firmly based argument can be used to derive the form of $g(\Delta_0)$. Δ_0 varies exponentially with the barrier height and separation. If the exponent is assumed to vary smoothly on the scale of kT_g, the form of $g(\Delta_0)$ is determined by the exponential dependence of Δ_0 on the barrier parameters:

$$g(\Delta_0) \propto \frac{1}{\Delta_0} \quad . \qquad 1.15$$

Some care should be taken not to assume that this form of $g(\Delta_0)$ is always (or even sometimes) valid. There is little direct experimental evidence in support of this precise form and indeed other slightly modified forms have been suggested. However, the use of eq. 1.15 allows a preliminary comparison to be made between experiment and theory.

The density of states n(E) can be calculated from $f(\Delta)$ and $g(\Delta_0)$. The details of this calculation involves a treatment of the singularities introduced by integrating 1.15 and will be discussed later in connection with time-dependent heat capacities, but as might be expected the result is a slowly varying logarithmic function of energy. The origin of the 'linear' temperature dependent term can be seen if this slight energy dependence is neglected, so that $n(E) \approx n_o$, a constant. The heat capacity is

$$C(T) = n_o \int_0^\infty \left(\frac{E}{2kT}\right)^2 \operatorname{sech}^2 \frac{E}{2kT} \, dE \qquad 1.16$$

where the integrand represents the response of a single two-level-system. Integration gives

$$C(T) = \frac{\pi^2}{6} n_o k^2 T, \qquad 1.17$$

a result that can be used to estimate n_o.

2. PHENOMENOLOGICAL THEORY

2.1 Transition Probabilities and Relaxation Times

Transitions between the states ψ_1 and ψ_2 occur through the perturbation of the potential well of Fig. 1.6a by a photon or phonon with energy $\hbar\omega = E$. This perturbation can change Δ or Δ_o (or both) but, of the two, changes in Δ are much more important.

The reason for this is twofold. The first is that the wavelength of the perturbing electric or strain field is much greater than the separation of the wells. As in the electric dipole approximation in semiclassical radiation theory, this leads to a perturbing potential which is essentially antisymmetric, equivalent to a change in Δ and not in Δ_o. Secondly, the matrix elements, calcualted in the localised basis $|1\rangle$ and $|2\rangle$, are relatively much smaller for a symmetric perturbation. (The use of the words symmetric and antisymmetric is of course not exactly correct, because the potential well of Fig. 1.6a is not symmetric. It is, however, a useful approximation, identifying perturbations that tend to change Δ or Δ_o separately.)

The second effect can be illustrated by comparing the matrix elements for two perturbing potentials Ax and Bx^2 for the one-dimensional double harmonic oscillator of Fig. 1.6a with $\Delta = 0$. The appropriate quantity for comparison is the ratio of the matrix element to the change in energy of each well ($Ad/2$ and $Bd^2/4$ in the two cases, where d is the separation of the minima). For the antisymmetric perturbation this ratio is ± 1 for the diagonal matrix elements and zero for the off-diagonal. In the case of the symmetric perturbation Bx^2 the diagonal elements are equal in both magnitude and sign and so give simply a shift in the zero of energy, while the ratio of the off-diagonal matrix elements to $Bd^2/4$ is $(\hbar\omega_o/4V)\exp(-2V_o/\hbar\omega_o)$. $V_o/\hbar\omega_o$ is considerably greater than unity for the low temperature application of this model, and so the off-diagonal terms in the $|1\rangle$, $|2\rangle$ basis can be neglected [notice that for $\Delta = 0$ the functions ψ_1 and ψ_2 defined by (1.11) and (1.12) are orthogonal, and so no particular precautions need be taken in the calculation].

The result has general validity. If the potential wells are not equivalent, or if Δ is not equal to zero, the antisymmetric perturbation will give off-diagonal terms and the symmetric perturbation will give, in addition to the off-diagonal terms, unequal diagonal terms. However, all these matrix elements are proportional to a factor of the general form $\exp(-2V_o/\hbar\omega_o)$ and so will be relatively unimportant, The perturbation to be included in the Hamiltonian (1.4) is therefore diagonal in the basis $|1\rangle$, $|2\rangle$. Using the transformation defined by (1.11) and (1.12), the perturbation in the ψ_1, ψ_2 basis has the form

$$\begin{pmatrix} \cos 2\theta & \sin 2\theta \\ \sin 2\theta & -\cos 2\theta \end{pmatrix} \text{or} \begin{pmatrix} \Delta/E & \Delta_o/E \\ \Delta_o/E & -\Delta/E \end{pmatrix} .$$

The interaction Hamiltonian can therefore be written in terms of the Pauli operators as

$$H_{int} = \left(\frac{\Delta}{E}\sigma_z + \frac{\Delta_o}{E}\sigma_x\right)p_o \cdot F + \left(\frac{\Delta}{E}\sigma_z + \frac{\Delta_o}{E}\sigma_x\right)\gamma e \qquad 2.1$$

in the presence of an electric field F and a strain field e. p_o and γ are defined as $1/2\partial\Delta/\partial F$ and $1/2\partial\Delta/\partial e$ respectively, and are therefore also equal to the eletric and elastic dipole moments of the equivalent classical potential. The vector character of F is here preserved, but the quantity γe has been written as an average over orientations (it can also be averaged over polarizations, although transverse and longitudinal models are usually considered separately). The off-diagonal term σ_x produces transitions between ψ_1 and ψ_2 while the diagonal term σ_z changes their relative energies.

In the simpler two-level system model the relationship between the diagonal and off-diagonal terms is ignored. The interaction Hamiltonian becomes

$$H_{int} = \left(\frac{1}{2}D\sigma_z + M\sigma_x\right)e + \left(\frac{1}{2}\mu\sigma_z + \mu'\sigma_x\right)F \qquad 2.2$$

where the diagonal and off-diagonal terms are specified independently.

The interaction between tunneling states of two-level systems and photons can conveniently be described by the use of the Einstein coefficients. Consider first the interaction of two-level systems with thermal phonons. Each two-level system is continually absorbing and emitting thermal phonons. The rate equation for the probability p_1 of finding the system in the ground state ψ_1 can be written

$$\frac{dp_1}{dt} = -p_1 B\rho(E) + p_2[A + B\rho(E)] \qquad 2.3$$

where A and B are phonon Einstein coefficients and $\rho(E)$ is the phonon energy density (per unit volume) evaluated at an energy E equal to the two-level system energy. $\rho(E)$ is given in terms of the density of states g(E) by

$$\rho(E) = \frac{Eg(E)}{e^{E/kT} - 1} . \qquad 2.4$$

In thermal equilibrium $dp_1/dt = 0$, and since $p_1 + p_2 = 1$

$$\frac{A}{B} = Eg(E) \quad . \tag{2.5}$$

For small departures from equilibrium eq. 2.3 defines a relaxation time τ, where

$$\tau^{-1} = [A + 2B\rho(E)] \quad , \tag{2.6}$$

which can be rewritten using eq. 2.4 as

$$\tau^{-1} = A \coth(E/2kT) \quad . \tag{2.7}$$

$1/A$ is the natural lifetime of the system at absolute zero, and at any temperature $\hbar\tau^{-1}$ is the uncertainty in the energy E.

The analysis can be continued to calculate the rate at which phonons are scattered by the two-level systems. If the density of states of the two-level systems is n(E) per unit volume, the change in the phonon energy density is given by

$$\frac{\partial\rho(E)}{\partial t} = E\, n(E)\, \frac{\partial p_1}{\partial t} \tag{2.8}$$

so that using eq. 2.3

$$\frac{\rho(E)}{dt} + n(E)BE(p_1 - p_2)\rho(E) = n(E)EAp_2 \quad .$$

The phonon lifetime is given by

$$\tau_{ph}^{-1} = n(E)BE(p_1 - p_2) = \frac{n(E)A}{g(E)} \tanh(E/2kT) \quad . \tag{2.9}$$

The coefficient B can be calculated starting from eq. 2.11 using a derivation equivalent to that of the corresponding optical problem. However, unlike the optical case, the form chosen for the density of states g(E) must be specified for phonons, as must the polarization. The Debye approximation can be used at temperatures of 1 K and below, so that the phonon density of states has a quadratic dependence on energy. Further, the phonon polarization can be classified as either longitudinal *l* of transverse *t*. For a single polarization α, B is given by

$$B = \frac{\pi M_\alpha^2}{\hbar\rho_o v_\alpha^2} \tag{2.10}$$

where ρ_o is the density of the solid and v_α is the velocity of sound for polarization α. M, as discussed in connection with eq. 2.1, is an average over orientations. The relaxation times can now be written for the *two-level system* as

$$\tau^{-1} = \sum_\alpha \frac{M_\alpha^2}{v_\alpha^5} \frac{E^3}{2\pi\rho_o\hbar^4} \coth(\frac{E}{2kT}) \tag{2.11}$$

and

$$\tau_{ph}^{-1} = \frac{\pi M_\alpha^2}{\hbar\rho_o v_\alpha^2} n(E)E \tanh(\frac{E}{2kT}) \tag{2.12}$$

where both longitudinal and transverse contributions have been included in the expression for τ^{-1}, but τ_{ph}^{-1} is written for a single polarization α.

For the *tunneling states* these formulae must be modified to take account of the explicit form of M_α. The tunneling state relaxation time is

$$\tau^{-1} = \Sigma \frac{\gamma_\alpha^2}{v_\alpha^5} \frac{\Delta_o^2 E}{2\pi\rho_o\hbar^4} \coth(\frac{E}{2kT}) \tag{2.13}$$

but the expression for the phonon scattering time is more complicated because, for a given phonon energy E, each tunneling state scatters phonons at a rate determined by M_α^2, proportional to Δ_o^2. In an amorphous solid, as opposed to a crystal, there will in general be a wide range of local environments and hence a range of values of Δ_o. The exact expression for τ_{ph}^{-1} involves the distribution function for Δ_o but for the moment it is sufficient to write

$$\tau_{ph}^{-1} = \frac{\pi\gamma_\alpha^2}{\hbar\rho_o v_\alpha^2} \bar{n}(E)E \tanh(E/k2T) \tag{2.14}$$

where $\bar{n}(E)$ is an effective density of states. In principle, the coupling parameter γ_α also varies from tunneling state to tunneling state, and it too should be represented by an average, although this can be incorporated into $\bar{n}(E)$.

One important difference between the two-level system model and the tunneling-state model should be noticed. As described in section 1.4 the specific heat can be calculated from n(E). In the two-level system model the same parameter enters directly into the expression for τ_{ph}^{-1}, but in the tunneling model this is not so, and the relationship between the heat capacity and τ_{ph}^{-1} depends on an unknown distribution function.

A description of absorption and emission in terms of the Einstein coefficients and semiclassical radiation theory is obviously oversimplified, and it is important to consider the extent to which it is valid. The semiclassical approach can be replaced by a quantized field calculation without changing the results. More important is the neglect in the Einstein treatment of coherence between the wave functions of the two energy levels.

The two-level system is here characterised by two parameters, the occupation probabilities, instead of the three that a full quantum treatment requires. This limitation means that the Einstein approach cannot provide a detailed explanation of non-linear and coherent effects (including higher-order transitions involved in Raman scattering). It does, however, give an accurate description of one-phonon or photon emission and absorption, although even simple scattering needs to be treated more carefully.

2.2 Heat Capacity

The results developed in section 2.1 can be used to discuss the dependence of the heat capacity on the time scale t_o of the measurement. It was mentioned in connection with the derivation of n(E) that the integration of $g(\Delta_o)$ needs care. The upper limit to Δ_o is obviously given by E, but in principle the lower limit is not well defined but depends on the way in which n(E) is measured. The time scale t_o of the experiment determines the minimum value of Δ_o through the formula for the relaxation time, eq. 2.13. Defining a distribution function $g(E,\tau)dE\,d\tau$, and writing it in terms of $f(\Delta)$ and $g(\Delta)$ gives (using eq. 2.13)

$$g(E,\tau)dE\,d\tau = f(\Delta)\,g(\Delta_o)\,\frac{\Delta_o E}{2\Delta\tau}\,dE\,d\tau \quad . \qquad 2.15$$

A minimum relaxation time τ_{min} is defined by putting $\Delta_o = E$ in eq. 2.13. Using $f(\Delta)$ constant, $g(\Delta_o) \propto 1/\Delta_o$ gives

$$g(E,\tau) = \frac{A}{\tau\left(1 - \frac{\tau_{min}}{\tau}\right)^{\frac{1}{2}}} \quad . \qquad 2.16$$

Equation 2.16 can in turn be used to give the density of states

$$n(E) = A\int_{\tau_{min}}^{t_o} \frac{d\tau}{\tau(1 - \tau_{min}/\tau)^{\frac{1}{2}}} = A\ell n(4t_o/\tau_{min}) \quad . \qquad 2.17$$

The tunnelling model therefore predicts not only that there is a wide distribution of relaxation times but also that the heat capacity depends on the time scale t_o on which it is measured. Of course, the precise forms of eqs 2.16 and 2.17 depend on the form chosen for $g(\Delta_o)$.

Over the last few years considerable effort has been devoted to experimental verifications of these predictions. The existence of a wide range of relaxation times has been conclusively demonstrated, but until recently the measurements of the heat capacity on short time scales have been unreliable and contradictory. The two most recent experiments indicate the kind of information that can now be obtained.

If a sample of glass at a temperature T_1 is suddenly connected to a thermal reservoir at temperature T_o ($T_o > T_1$) by a thermal link of conductance α, in the absence of a distribution of relaxation times the temperature of the sample will decrease exponentially with time. As the temperature of the sample approaches T_o, the temperature-time curves can be superposed as shown in Fig. 2.1. The observed behaviour is quite different: as shown in Fig. 2.2 the temperature varies much more slowly with time than in Fig. 2.1.

These results can be understood on the basis of an idealized model of the experiment. The rate at which heat is evolved from the sample is given by $\alpha\dot{T}$ and at long times this will be the result of the slow evolution of energy from tunnelling states with long relaxation times. Ordinary phonons relax rapidly and can be neglected except in so far as they define the temperature. Using the distribution function defined in eq. 2.16 the instantaneous rate of energy loss is

$$\dot{Q} = \int_{kT_o}^{kT_1}\int_{\tau_{min}}^{\infty} \frac{E}{\tau}\,g(E_1\tau)\,e^{-t/\tau}\,dEd\tau \quad . \qquad 2.18$$

This can be integrated if $t \gg \tau_{min}$ (which is certainly true) to give

$$\dot{Q} = \frac{Ak^2}{2t}\,(T_1^2 - T_o^2) \quad . \qquad 2.19$$

Equation 2.19 agrees well with the results and illustrates an important aspect of the amorphous state. Amorphous solids contain a large range of relaxation times and under very general assumptions (such as those outlined in connection with eq. 15) this leads to non-exponential relaxation. In particular, integration of functions similar to that used in eq. 2.13 leads to relaxation as $1/t$.

The main conclusion of the experiments shown in Fig. 2.2 is that there is a broad distribution of long ($50s < \tau < 5000s$) relaxation times, in agreement with low frequency acoustic measurements. A probe of much shorter relaxation times is provided by heat pulse propagation. A pulse of heat is applied to one side of a thin glass slide, and the temperature is monitored as a function of time at the other. By comparing the temperature-time response with solutions of the diffusion equation, a value for the heat capacity on a time scale corresponding to the thermal diffusion time can be measured. Values of this characteristic time varying from 1 μs to a few seconds have been obtained by using slides of different thicknesses. The results of two of these studies are shown in Fig. 1.3, where the decrease in heat capacity is clear. However this figure demonstrates equally well the uncertainty of the results. At least five sets of experiments have been performed, with

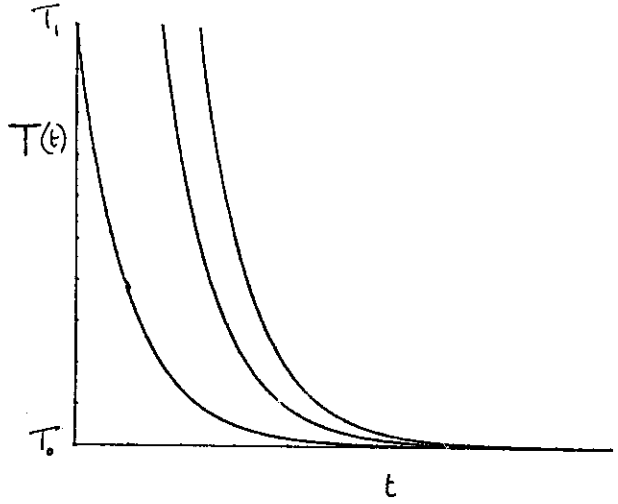

2.1 Exponential decays expected on cooling from different initial temperatures to T_0 if no relaxation effects are present.

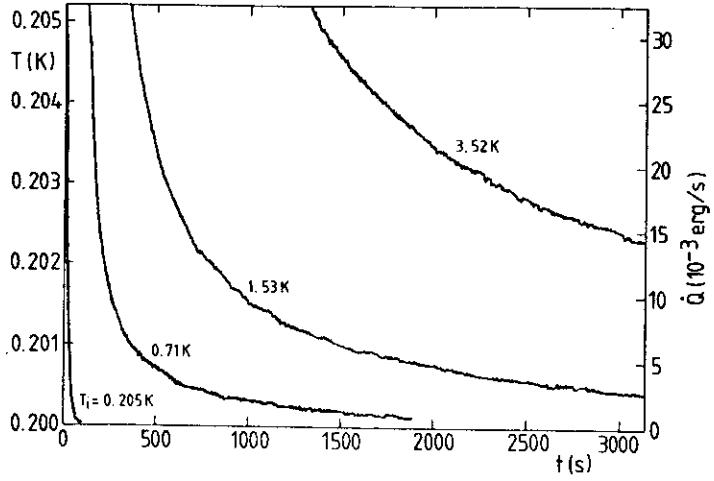

2.2 Thermal relaxation in vitreous silica between 0.205 and 0.200 K. (J. Zimmermann and G. Weber, Phys. Rev. Lett., 46, 661, 1981.)

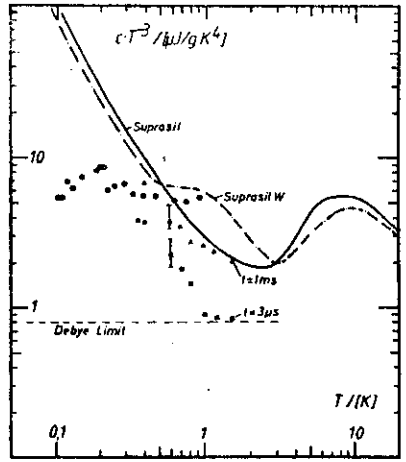

2.3 Heat capacity of vitreous silica measured on different time scales. (M. Meissner and K. Spitzmann, Phys. Rev. Lett., 46, 265, 1981.)

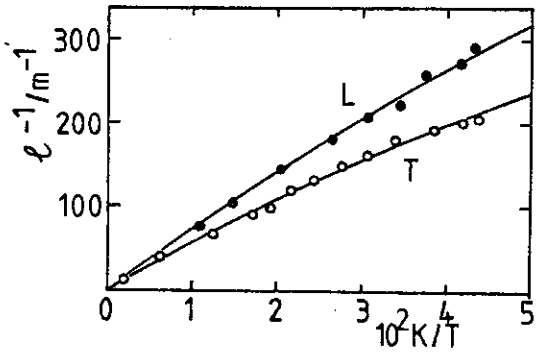

2.4 Temperature dependence of the measured phonon free path. The solid curves are $\ell^{-1} = \ell_0^{-1} \tanh \hbar\omega/2kT$ (after B. Golding, J.E. Graebner and R.J. Shutz, Phys. Rev., B14, 1660, 1976).

inconsistent results, although all show the existence of relaxation time effects.

2.3 Phonon Scattering

The phonon scattering time defined in eq. 2.14 can be applied both to thermal conductivity and to acoustic experiments. In general the acoustic experiments are used to measure the parameter $\bar{n}\,\gamma^2$ (and v) which can then be used to calculate the thermal conductivity below 1 K.

The temperature dependence of κ follows from application of the dominant phonon approximation to eqs 1.1 and 2.14. This approximation states that at a temperature T the relevant phonons are those for which $\hbar\omega \sim kT$. The temperature dependence of τ_{ph} is obtained by putting $E = \hbar\omega \sim kT$, so $\tau_{ph} \propto 1/T$. Together with the T^3 variation of C this gives the T^2 dependence of κ. A more careful treatment involves not only the use of the real energy dependent density of states $\bar{n}$ in eq. 2.14 but also a generalization of eq. 1.1 to include an integration over all phonon frequencies. Such a calculation reproduces the experimental results more exactly, and shows why the observed temperature dependence of κ is $T^{1.9}$ and not T^2.

Equation 2.14 has been extensively tested by means of acoustic experiments at low powers. At acoustic frequencies the condition $\hbar\omega << kT$ is satisfied at all but the lowest temperatures so that $\ell_{ph}^{-1} \propto \omega^2/T$, the attenuation increasing at lower temperatures as shown in Fig. 1.5. In fact the complete expression 2.14 has been shown to give a good description of the low power attenuation, as shown in Fig. 2.4.

Associated with this attenuation is a temperature dependent acoustic velocity. Applying the Kramers-Kronig equations to the acousitc case gives a value for this contribution Δv to the velocity

$$\Delta v = \frac{P}{\pi} \int_0^\infty \frac{v\tau_{ph}^{-1}\, d\omega'}{\omega^2-\omega'^2} \quad . \qquad 2.20$$

Relative to a reference temperature T_o the change in velocity is given in the limit $\hbar\omega << kT$, using eq. 2.14, by

$$v(T) - v(T_o) = \frac{\bar{n}\gamma^2}{\rho v} \ln(T/T_o) \quad . \qquad 2.21$$

Experimental results, as illustrated in Fig. 2.5, confirm this behaviour and give values for the product $\bar{n}\gamma^2$. The logarithmic dependence of the velocity is a characteristic feature of tunnelling states and has been used to show the existence of such states in materials, such as amorphous metals, where the contribution of tunnelling states to the thermal properties is difficult to identify.

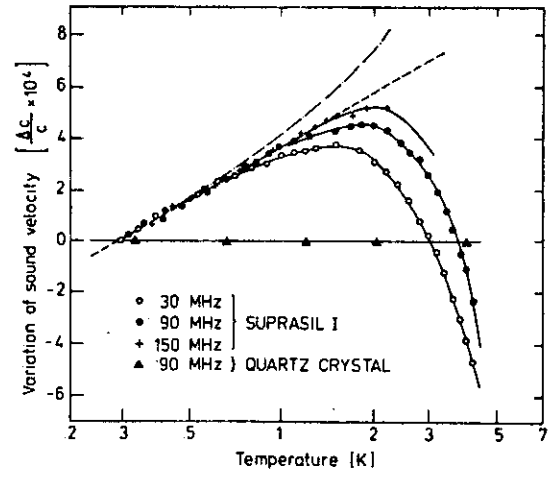

2.5 Acoustic velocity as a function of temperature in silica. (L. Piché, R. Maynard, S. Hunklinger and J. Jäckle, Phys. Rev. Lett., 32, 1426, 1974.)

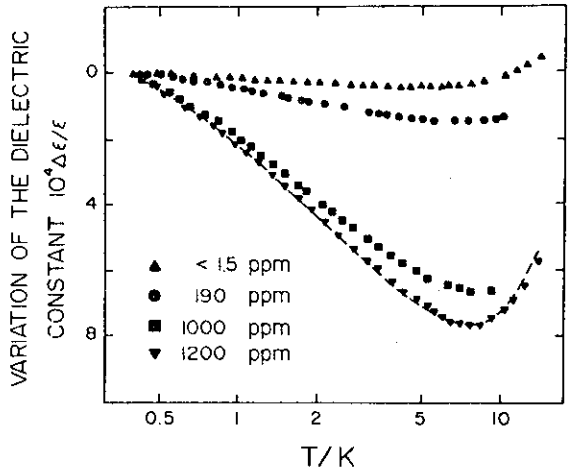

2.6 Temperature dependence of the dielectric constant for vitreous silica containing different concentrations of OH. (S. Hunklinger and M. v Schickfus, J. Phys. C., 9, L439, 1976.)

Perhaps the most important feature of the acoustic experiments is the phenomenon of saturation. This can be readily understood on the basis of the Einstein treatment. Implicit in eq. 2.4 is the fact that transitions are induced by phonons from a thermal distribution. At larger acoustic powers this will no longer be the case, and $\rho(E)$ in eq. 2.3 will be determined by the acoustic phonon flux. As this increases spontaneous transitions become relatively unimportant, and the populations of the two-levels will both tend to one half. Stimulated emission processes therefore compensate for the absorption, and there is very little net attenuation. An estimate of the acoustic power at which this occurs can be obtained by equating the thermal phonon and acoustic phonon concentrations.

Although this appears straightforward one point requires clarification. The thermal phonon concentration can be expressed per unit frequency (or energy) range, but a calculation of the corresponding acoustic phonon concentration requires a knowledge of the effective bandwidth. This can be determined either by the length of the acoustic pulse (i.e. an experimental broadening) or by the intrinsic lifetime of the tunnelling state. This has been mentioned previously in connection with eq. 2.7, and will be discussed in much more detail later. At this point it is sufficient to say that most information is obtainable in the continuous wave limit, where the effective bandwidth is intrinsic. In this case, if the number of acoustic phonons per unit frequency range is equated to the number of thermal phonons, the critical energy density E_c is given by

$$\frac{E_c}{\hbar\omega\ T_2^{-1}} = \frac{\omega^2}{\pi v^3}\ \frac{kT}{\hbar\omega}\ ,$$

where T_2^{-1} is the line width of the tunnelling state and the final factor comes from the low frequency expansion of the Bose factor. This gives

$$E_c = \frac{\omega^2 kT}{\pi\ v^3 T_2}$$

or equivalently for the power density J_c (W m^{-2})

$$J_c = \omega^2 kT/\pi v^2 T_2 . \qquad 2.22$$

The results shown in Fig. 2.6 imply a value of roughly 10 ns for T_2, but this is not the value predicted by eq. 2.13 in general. Interaction between tunnelling states gives a line width T_2^{-1} greater than that predicted from the relaxation time T_1.

2.4 Dielectric Absorption

There is an exact parallel between the absorption of electromagnetic and acoustic waves. The dielectric absorption varies in the same way as the acoustic attenuation, and the velocity of light in the glass (or the dielectric constant) varies logarithmically with temperature. Results in vitreous silica are shown in Fig. 2.6.

The main difference between the electronmagnetic and acoustic results lies in the sample dependence of the results. In the acoustic case all samples of SiO_2, for example, give the same value for $\bar{n}\gamma^2$, but the measurements of dielectric constant represented in Fig. 2.6 show an effect proportional to the concentration of water (or hydroxyl ions) in the silica. This is not unexpected in view of the large dipole moment of hydroxyl, but is clear evidence of the rôle of impurities in some of these phenomena.

2.5 Thermal Expansion

Although the range of experimental data is limited, the thermal expansion β of glasses at low temperatures reflects the other unusual thermal properties. Results in vitreous silica are shown in Figs 2.7 and 2.8. The Gruneisen parameter used to describe the expansion is defined from the experimental results as $\beta V/\chi_T C_V$ where χ is the isothermal compressibility. This parameter balances the strong temperature dependencies of β and C_V to give a quantity which varies slowly with temperature, and which is of order +1 in ordinary crystalline solids. Microscopically, it is a measure of the variation of the frequencies of the excitations with volume, $-\partial \ell n\omega/\partial \ell nT$, as can be seen from a quasi-harmonic treatment. The vibrational frequencies are assumed to vary with volume but not explicitly with temperature, so that the entropy S can be written as $S(\omega(V)/T)$. Then

$$\left(\frac{\partial S}{\partial V}\right)_T = \frac{1}{T}\ S'\left(\frac{\partial \omega}{\partial V}\right)_T$$

and

$$\left(\frac{\partial S}{\partial T}\right)_V = -\ \frac{\omega S'}{T^2}\ .$$

Using $C_V = T(\partial S/\partial T)_V$ and rearranging gives

$$\left(\frac{\partial S}{\partial V}\right)_T = -\ \frac{C_V}{\omega}\left(\frac{\partial \omega}{\partial V}\right)_T\ .$$

Now

$$(\partial S/\partial V)_T = -\ (\partial P/\partial V)_T(\partial T/\partial V)_P\ ,$$

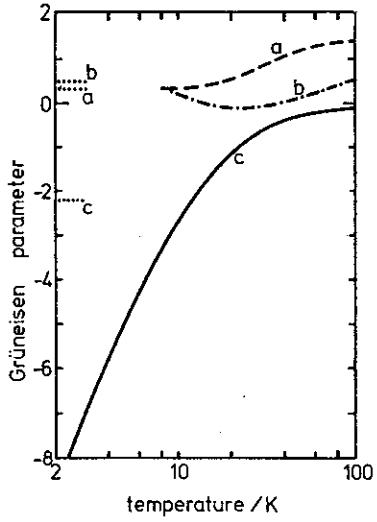

2.7 Gruneisen parameter as a function of temperature for a) KCℓ, b) crystalline germanium and c) vitreous silica. The dotted lines give the limiting value calculated from the pressure derivatives of the sound velocities (W.A. Phillips, Ref 1).

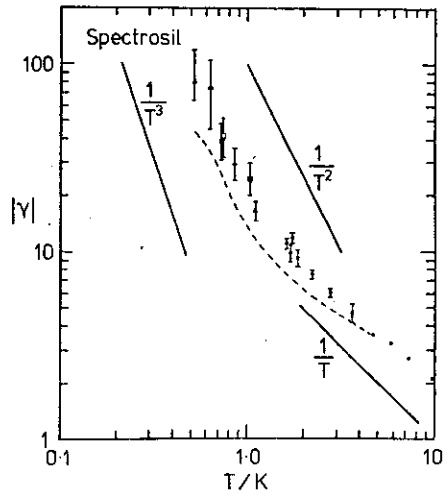

2.8 Gruneisen parameter as a function of temperature below 10 K (O.B. Wright, Thesis, 1982).

so

$$\beta V/\chi_T C_V = - \partial \ell n\omega/\partial \ell nV \quad .$$

This means that an explanation of the large negative Gruneisen parameter at 1 K or below requries a demonstration that the total energy of the tunnelling states decreases dramatically as the volume of the solid is decreased.

Although no detailed explanation has been attempted it is possible to see two ways in which this might occur. Firstly, the tunnel splitting Δ_o is exponentially dependent on the barrier height and the separation of the two potential minima. If these parameters are sensitive to volume changes (as they are in the case of tunnelling defects in crystals) a large change in Δ_o and hence in the energy of the tunnelling state will result. The main problem with this explanation is that for most states of a given energy E, $\Delta_o \ll E$.

The second possible explanation involves the large coupling of these states to strain fields. A typical coupled constant of 1 eV gives a value of 10^4 for $\partial \ell n\omega/\partial \ell nV$. Although this value for a single state is enormous, states are at first sight equally likely to increase in energy as to decrease, and it is difficult to see how a large resultant value can be obtained.

3. DYNAMICS OF TWO-LEVEL SYSTEMS

3.1 Quantum Treatment

The Einstein analysis presented in 2.1 neglects an important aspect of the quantum mechanical theory of two-level systems, the coherence between the wavefunctions describing the two states. A simple analysis will be used in this section to show that additional detailed information can be obtained from echo experiments which explore this coherence.

If an alternating electric field is applied to a two-level system the Hamiltonian is of the form

$$H = H_o + H_1(t)$$

where H_o has eigenfunctions ψ_1 and ψ_2 satisfying

$$H_o\psi_1 = -\frac{E}{2}\psi_1 \quad \text{and} \quad H_o\psi_2 = +\frac{E}{2}\psi_2$$

and $H_1(t) = -2e \times \varepsilon_o \cos \omega t$. The general solution of

$$H\Psi = i\hbar \frac{\partial \Psi}{\partial t}$$

can be written

$$\Psi = c_1(t)\ \psi_1\ e^{i\omega_o t/2} + c_2(t)\ \psi_2\ e^{i\omega_o t/2} \qquad 3.1$$

where $\hbar\omega_o = E$. Substituting this solution in Schrodinger's equation gives

$$\begin{aligned} &H_{11}\ c_1(t) + H_{12}\ e^{-i\omega_o t}\ c_2(t) = i\hbar\dot{c}_1(t) \\ \text{and} \qquad &H_{21}\ e^{i\omega_o t}\ c_1(t) + H_{22}\ c_2(t) = i\hbar\dot{c}_2(t) \end{aligned} \qquad 3.2$$

where $H_{ij} = \langle\psi_i|H_1(t)|\psi_j\rangle$.

In the amorphous solid, containing a broad distribution of frequencies ω_o, some states will always be in resonance for any driving frequency ω: the frequency of the electric field selects a small number of two-level systems from the distribution. The most important terms on the left of eqs 3.2 are therefore those for which $\omega = \omega_o$ and which give a time independent contribution to $\dot{c}_1$ and $\dot{c}_2$. The rapidly varying terms can be neglected just as they are in the analagous discussion of magnetic resonance. In addition, since from eq. 2.13 the strongest coupling between tunnelling states of energy E and photons (or phonons) occurs in the symmetric case when $\Delta_o = E$, the discussion can be limited to these almost symmetric states for which H_{11} and H_{22} are very small. With these assumptions eqs 3.2 become

$$\begin{aligned} H_1^o\ c_2 &= i\hbar\dot{c}_1 \\ H_1^o\ c_1 &= i\hbar\dot{c}_2 \end{aligned} \qquad 3.3$$

where $H_1^o = -\langle\psi_1|e\varepsilon_o x|\psi_2\rangle = -\varepsilon_o p'$, defining the induced dipole moment p'. Combining the two eqs 3.3 gives equations for c_1 and c_2 of the form

$$\ddot{c}_1 = -\frac{\varepsilon_o^2 p'^2}{\hbar^2}\ c_1 = -\omega_1^2 c_1 \qquad 3.4$$

with solutions $e^{\pm i\omega_1 t}$.

In all experiments involving coherence the sample must initially be in a well defined state, and in amorphous solids this is achieved by keeping the sample as cold as possible (10 mK). A basic experiment consists of applying two pulses of r.f. electric field, the first of length τ and the second, a time t_o later, of length 2τ. If the two-level system is initially in the state ψ_1 the appropriate solution during the first pulse is

$$\Psi(t) = \psi_1\cos\omega_1 t + \psi_2\sin\omega_1 t \quad . \qquad 3.5$$

The pulse length (or the magnitude of ε_o) is chosen so that $\omega_1\tau = \pi/4$, or

$$\frac{2\varepsilon_o p'\tau}{h} = \frac{\pi}{2} \qquad 3.6$$

(a $\pi/2$ pulse) so that at the end of the pulse the state of the system is described by

$$\psi(\tau) = \frac{1}{\sqrt{2}}(\psi_1 + \psi_2) \quad . \qquad 3.7$$

For the symmetric case, the combination (3.7) corresponds to a state which instantaneously has a large dipole moment, in contrast to the states ψ_1 or ψ_2 which do not. This large dipole moment can be detected experimentally.

During the time interval between the pulses the evolution of the state function can be followed in the usual way for time independent problems, so that at time t_o after the first pulse ($t_o \gg \tau$)

$$\psi(t_o) = \frac{1}{\sqrt{2}}(\psi_1\ e^{+i\omega_o t_o/2} + \psi_2\ e^{-i\omega_o t_o/2}) \quad . \qquad 3.8$$

The second pulse acts exactly as the first, except that the phase change $\omega_1 t$ during the pulse is $\pi/2$ instead of $\pi/4$. Choosing solutions of eq. 3.4 to match eq. 3.8 gives

$$\Psi(t) = \frac{1}{\sqrt{2}}((\psi_1\cos\omega_1 t + \psi_2\sin\omega_1 t)e^{i\omega_o t_o/2} + (\omega_1\sin\omega_1 t + \psi_2\cos\omega_1 t)e^{-i\omega_o t/2}) \qquad 3.9$$

$$t_o < t < t_o + 2\tau \quad .$$

At the end of the pulse

$$\Psi(t_o+2\tau) = \frac{1}{\sqrt{2}}\left(\psi_2 e^{i\omega_o t_o/2} + \psi_1 e^{i\omega_o t/2}\right) \qquad 3.10$$

and at a later time t, again taking $t \gg \tau$,

$$\Psi(t + t_o) = \frac{1}{\sqrt{2}}\left(\psi_2 e^{i\omega_o (t_o-t)/2} + \psi_1 e^{-i\omega_o (t_o-t)/2}\right) . \qquad 3.11$$

Equation 3.11 shows that at a time t_o after the second pulse the system is again in the state

$$\Psi = \frac{1}{\sqrt{2}}(\psi_1 + \psi_2)$$

with a large dipole moment. More importantly this is true for all values of ω_o. In an amorphous solid, as a result of the finite lifetime of the states and the finite length of the exciting pulse, the electric field will inevitably excite states with a range of energies or frequencies ω_o. The effect of this is to give a very sharp 'echo' t when eq. 3.11 is averaged over a range of ω_o. It is interesting that the broad distribution of energies is responsible for this sharpness of the echo.

3.2 Echo Experiments

This analysis assumes that the phase coherence of the state function is maintained for the complete time $2t_o$. Any disruption of this phase coherence will prevent a tunnelling state from contributing to the final echo, and therefore the experiment provides a way of measuring the dephasing time, known as T_2. The echo amplitude in this simple picture is expected to decrease as $\exp(-2t_o/T_2)$, and T_2 can be determined by measuring the echo amplitude as a function of t_o.

These experiments, in which two pulses of acoustic or electric fields are used to measure T_2, are known as spontaeous echo experiments. In the ideal photon case two electric field pulses of length τ and 2τ (typically 1 μs) at a frequency $\omega/2\pi$ of about 1 GHz are applied to a sample held at a temperature T of a few mK, where $\hbar\omega > kT$. This low temperature is needed in order to prepare the system in the ground state ψ_1. The amplitude of the echo is measured as a function of the electric field amplitude ϵ_o at fixed pulse separation t_o, and also as a function of t_o at fixed ϵ_o. A typical echo pattern is shown in Fig. 3.1.

Results typical of electric echo experiments are shown in Fig. 3.2. The maximum in the echo amplitude as a function of ϵ_o corresponds from eq. 3.6 to $\pi/2$ and π pulses or $\epsilon_o \tau p'/\hbar = \pi/4$, and can be used to evaluate p'. It

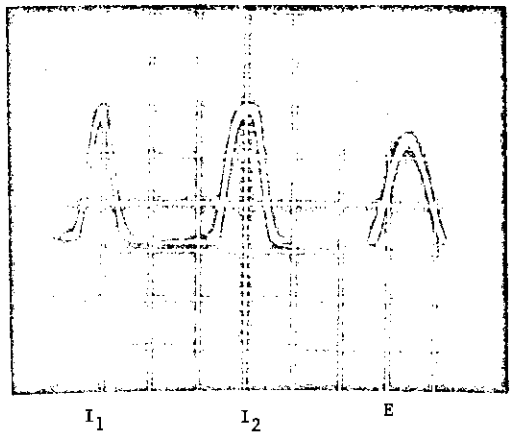

3.1 Spontaneous electric echo, pattern (L. Bernard, Thèse, Grenoble, 1979).

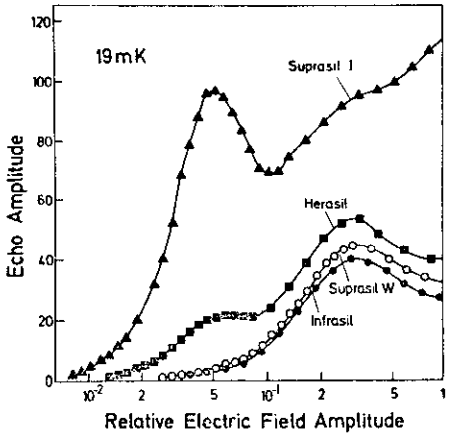

3.2 Amplitude of the spontaneous electric echo in vitreous silica samples, plotted as a function of electric field. (B. Golding, M. v Schickfus, S. Hunklinger, K. Dransfeld, Phys. Rev. Lett., 43, 1817, 1979.)

is clear from Fig. 3.2 that two distinct species of dipole occur in these glasses, and by choosing ε_o appropriately each type can be studied in turn. A number of complications, including the random orientation of the dipoles relative to the field and the problem of determining the local field, make precise values of p' difficult to determine, but values are typically of order 3×10^{-30} Cm (1 Debye). The corresponding phonon experiment in silica gives values for the coupling constant γ of about 1 eV.

The variation of the echo amplitude with t_o is shown in Fig. 3.3 for a pulse area which corresponds to the first peak of Fig. 3.2 (which turns out to be the result of OH groups). An exponential variation is found in this case, although in general more complicated patterns of decay are observed. These non-exponential decays may result from a distribution of relaxation times similar to that discussed in section 2.2, but could also be characteristic of the molecular process responsible for T_2, to be discussed in section 3.3. The results shown in Fig. 3.3 show that T_2 is about 70 μs at 10 mK, and varies as T^{-1}. Phonon echo experiments show slightly smaller values of T_2, 10 μs at 20 mK, with a temperature variation of T^{-2}. These phonon experiments are probably observing the second set of states, but the different temperature dependences may well result from different experimental conditions.

More complicated three pulse sequences of electric and acoustic fields can be used to measure T_1 in 'stimulated' echo experiments. In one such experiment on initial π pulse is followed a time t_o later by π/2 and π pulses, relatively closely spaced. The analysis of this experiment follows that given in section 3.1. The system, initially in the ground state ψ_1, is excited coherently to the state ψ_2 by the first π pulse. During the time t_o a fraction e^{-t_o/T_1} of the systems will relax back to the ground state ψ_1. The double pulse sequence gives a spontaneous echo just as before, but the contribution of those systems which decayed back to ψ_1 will be opposite to that of the systems remaining in ψ_2. The amplitude of the echo will therefore be proportional to $1 - e^{-t_o/T_1}$ and measurements as a function of t_o can be used to measure T_1. Both photon and phonon measurements in vitreous silica give results in agreement with eq. 2.13, although this experiment is also affected by the wide distribution of tunnelling state relaxation times. Results of stimulated photon experiments are shown in Fig. 3.4. Measured values of T_1 are up to ten times larger than those of T_2.

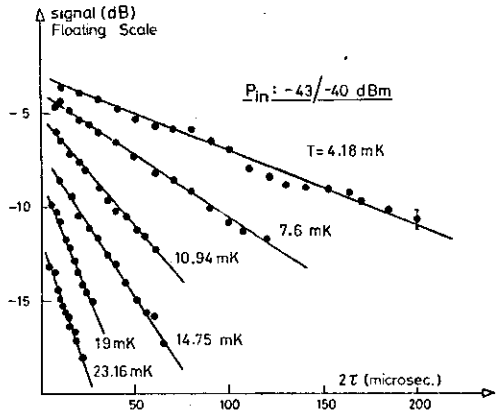

3.3 Decay of spontaneous electric echoes (L. Bernard, Thèse, Grenoble, 1979).

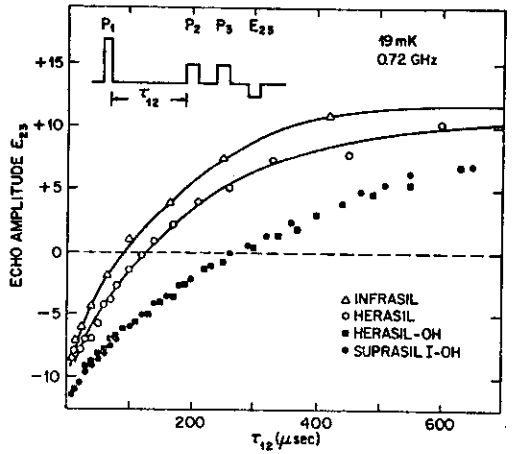

3.4 Amplitude of stimulated echo as a function of the time between initial and second pulse (B. Golding, M. v Schickfus, S. Hunklinger, K. Dransfeld, Phys. Rev. Lett., 43, 1817, 1979.)

3.3 Spectral Diffusion

A dephasing time T_2 much shorter than an energy relaxation time T_1 implies, by analogy with magnetic resonance, interaction between the two-level systems. This interaction could take two forms. The term proportional to σ_x in the Hamiltonain gives rise to a process in which two systems exchange energy by mutual excitation and de-excitation with exchange of a resonant phonon. In a glass, however, the density of resonant two-level systems lying within the band width of a pulse is too small for this to be an effective dephasing process. Much more effective is the non-resonant process involving σ_z in which a transition of one system, equivalent to a reorientation of an elastic dipole, gives rise to a strain field which affects the energy of a neighbour. Since all systems with energy less than about $2k_BT$ undergo such transitions the number of effective interactions is much greater.

A semiquantitative explanation of the effect can be given by means of a simple physical picture. Each system experiences a fluctuating local strain field which in equilibrium gives rise to a fluctuating energy ΔE_o as shown in the upper half of Fig 3.5. The initial field pulse, of duration less than the time scale of the fluctuations, selects from the distribution a subset which instantaneously have energy $E_o = \hbar\omega_o$. Because the mean energy of systems within this subset differ, the energies gradually spread out over a range determined by the fluctuating fields. This is illustrated in the lower half of Fig. 3.5b. At times long compared to the average relaxation time the width of the energy distribution of the subset reaches ΔE_o, and is then independent of time.

A value for ΔE_o can be evaluated from the strength of the coupling between the two-level systems and the phonons. The elastic dipole moment is γ so that the interaction energy is

$$\delta E \sim \frac{\gamma^2}{\rho v^2 r^3} \quad . \qquad 3.12$$

Replacing $1/r^3$ by the concentration of thermally excitable two-level systems gives

$$\Delta E_o \sim \gamma^2 \bar{n} k_B T/\rho v^2 \quad . \qquad 3.13$$

In the long time limit the time interval t_o between the two pulses of a spontaneous echo experiment is much greater than T_{1min}, defined as the shortest energy relaxation time for two-level systems with energy $E \sim k_BT$. The dephasing time can be derived as the time for which the spread in phase,

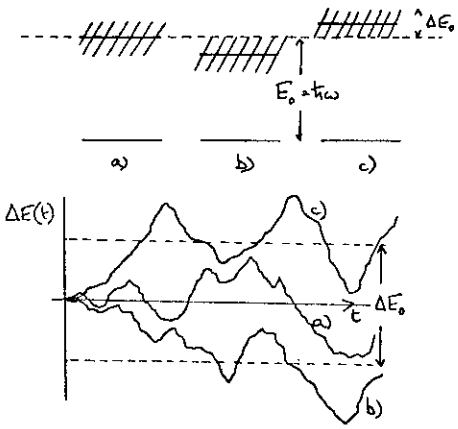

3.5 Representation of broadening arising from spectral diffusion.

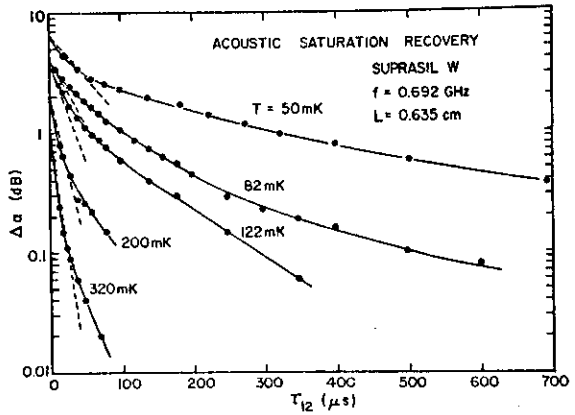

3.6 Attenuation of a weak probing pulse applied a time τ_{12} after a saturating pulse (B. Golding and J.E. Graebner, Ref 1).

$\Delta E_o t/\hbar$, is of order $\pi/2$. This gives

$$T_2^{-1} = \frac{\pi}{2}\frac{\Delta E_o}{\hbar} \simeq \frac{\pi\gamma^2 \bar{n} k_B T}{2\hbar\rho v^2} \qquad 3.14$$

and an exponential decay of the echo amplitude.

In the short time limit, $t_o << T_{min}$, the width of the energy distribution increases roughly as $\Delta E_o(1 - e^{-t/T_{min}})$, so

$$\Delta E(t) = \Delta E_o t/T_{min}. \qquad 3.15$$

This defines a dephasing time by

$$\frac{1}{\hbar}\int_o^{T_2} \Delta E(t)dt = \frac{\pi}{2}$$

so

$$T_2^2 = \hbar\pi T_{min}/\Delta E_o \quad . \qquad 3.16$$

The decay is non-exponential, varying with t_o as

$$\exp(-\Delta E_o t_o^2/\hbar T_{min}) \quad . \qquad 3.17$$

The dephasing time therefore varies with temperature as T for $t_o > T_{min}$ and as T^{-2} for $t_o << T_{min}$, using $T_{min} \propto T^{-3}$. Using numerical values for the constants in eq. 3.14 the value of T_2 at 20 mK can be estimated as 20 μs in vitreous silica if $\bar{n}\gamma^2$ is taken as 10^7 J m^{-3}, a value derived from acoustic velocity measurements of the kind shown in Fig. 2.5. This is in reasonable agreement with experiment.

It must be emphasized that many complications have been ignored in this simple argument. In particular the broad distribution of relaxation times T_1 complicates the analysis, and a rigorous derivation of eq. 3.17 is complicated. However, this analysis does show the underlying physical principles, and illustrates that this spectral diffusion can explain the observed interaction between two-level systems.

3.4 Saturation and Linewidth Experiments

The phenomenon of spectral diffusion can be probed by direct measurements of the linewidth of two-level systems, and indeed such experiments provided the first evidence that interaction between the systems is important. The ideal experiment uses a large intensity initial pulse to saturate a subset of two-level systems, followed by a second weaker pulse which monitors the recovery to thermal equilibrium. This second pulse may have the same frequency ω_o as the first, in which case the time delay between the two is

varied, or can be used to examine the frequency dependence. Interpretation of the various experiments depends critically on the relationship between the length τ of the saturating pulse, and the relaxation times T_1 and T_2.

Figure 3.6 shows saturation recovery experiments in vitreous silica, where τ_{12} is the time delay between the pulses, both a frequency ω_o. The temperature is sufficiently low for T_2 to be comparable to τ (0.06 μs), and both are much less than T_1. The initial pulse saturates a subset of two-level systems in a frequency band of width $\hbar/\tau$ at ω_o, comparable to the linewidth ΔE_o (Fig. 3.5). Spectral diffusion does not therefore have a large effect, and the second pulse monitors the recovery of equilibrium through energy relaxation, and hence measures T_1. The dashed lines in the figure correspond to a one phonon process with γ = 1.4 eV. At longer times the recovery shows a much slower time variation, reminiscent of the data shown in Fig. 2.2, and may be another illustration of the large range of relaxation times in glasses.

The intrinsic linewidth of the two-level systems can be measured by working in the limit $T_2 < \tau < T_1$, and measuring the saturation produced by an initial pulse of variable frequency ω at fixed intial frequency ω_o of the second. (For obvious experimental reasons it is better to keep the frequency of the second detected pulse constant.) Experimental results in vitreous silica are shown in Fig. 3.7. The width of the line is much larger than $\hbar/\tau$ or $\hbar/T_1$, giving additional evidence for interaction effects. In addition the dependence of linewidth on pulse length is direct evidence for the time evolution of the linewidth implied by spectral diffusion: the longer the pulse the broader the line (Fig. 3.5). A detailed comparision of linewidth results with the predictions of spectral diffusion theory is shown in Fig. 3.8.

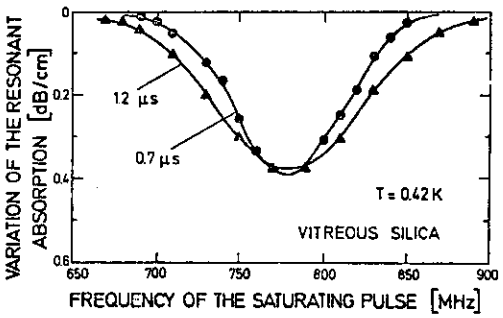

3.7 Attenuation of weak probing pulse as a function of saturation pulse frequency for two values of saturating pulse length. (W. Arnold, C. Martinon and S. Hunklinger, J. de Physique, C6, 961, 1978.)

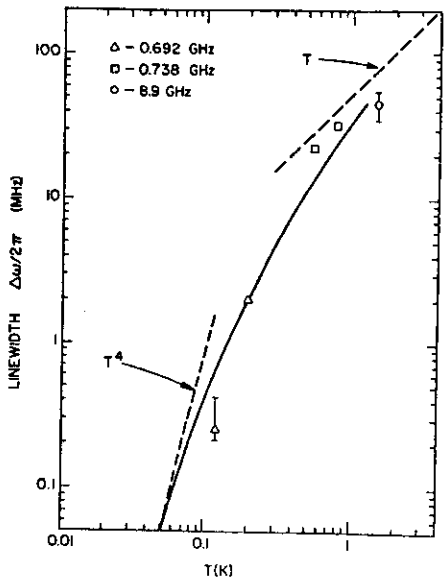

3.8 Linewidth obtained from saturation experiments plotted as a function of temperature (B. Golding and J.E. Graebuer, Ref 1).

4. MICROSCOPIC INTERPRETATIONS

4.1 Impurity Effects

It is clear that a wide range of thermal, acoustic and electrical measurements can be interpreted in terms of two-level systems, or, more specifically, in terms of a tunnelling model. The vast majority of the non-thermal experiments have been performed on vitreous silica, and have established many important parameters: the density of states, the dipole moment and the phonon coupling constant are all known. Much less is known about the properties of these states in other amorphous systems such as organic polymers, chalcogenide glasses or even other oxide glasses. Glassy metals have, however, been extensively studied and will be discussed in section 4.2.

Although experiments can be interpreted in terms of a general tunnelling model, such an approach leaves unanswered two important questions; what is the microscopic nature of the states and why do (almost?) all amorphous solids contain them? In particular one of the more important questions concerning the low temperature properties of glasses is whether the effects are intrinsic, in the sense that they would occur in a fully coordinated random network model of a glass, or whether defects, in the form of incomplete coordination, or water, must be present. To answer this it is helpful to look at the results shown in Fig. 4.1. Samples of As_2S_3 were prepared with increasing care and decreasing impurity concentrations. The concentrations of impurity in the two purest samples, determined by mass spectroscopy, were about 10^{24} m^{-3} of Ge and less than 10^{23} m^{-3}, respectively. Even so, both these samples showed an excess heat capacity, with the order of magnitude reduction in impurity concentration halving the excess heat capacity. The corresponding additional entropies can be evaluated, and on the assumption that two-level systems are involved, lead to *minimum* numbers of contributing states which are between 10^{23} m^{-3} and 10^{24} m^{-3} in both cases. It was concluded from the lack of proportionality between impurity level and heat capacity that an "intrinsic" tern would be left after removal of all impurities, although this is a slightly dangerous conclusion which depends crucially on the realiability of the chemical analysis. Measurements of κ in the two samples point to an intrinsic effect, since the values are the same within experimental error.

Other evidence is ambiguous. Measurements in the more highly coordinated amorphous solids As and Ge show a much smaller excess heat capacity, although the interpretation of these results is complicated by sample inhomogeneities. It appears, however, that the density of tunnelling states is less in these more rigid networks than in the glasses containing two-fold coordinated

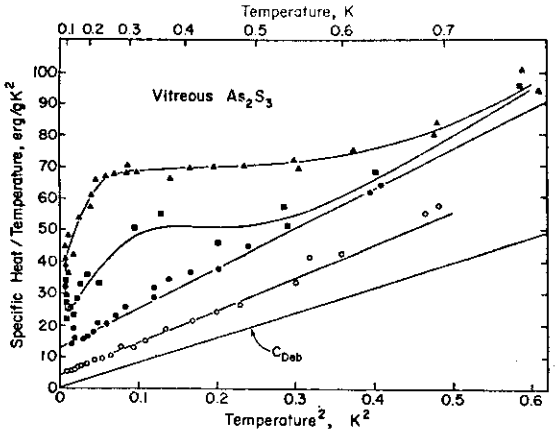

4.1 Heat capacity of As_2S_3. The heat capacity decreases as the purity increases (R.B. Stephens, Phys. Rev., B13, 852, 1976).

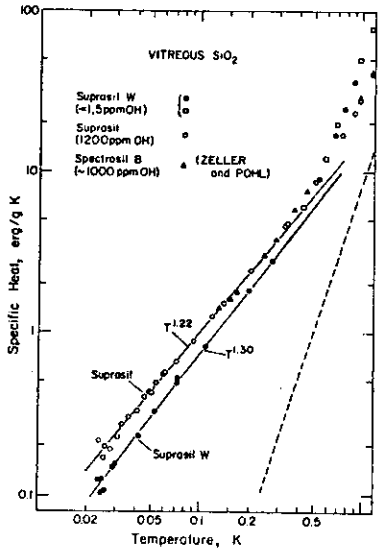

4.2 Heat capacity of vitreous silica containing 1 and 1200 ppm OH (J.C. Lasjaunias, A. Ravex, M. Vandorpe, and S. Hunklinger, Solid State Comm., 17, 1045, 1975).

atoms or groups of atoms.

The effect of one particular impurity, the hydroxyl group OH, has been studied in some detail. These studies not only identify one particular impurity which can change the low temperature properties, but also help to build up a picture of the microscopic structure of one possible tunnelling state as discussed in section 4.3. Fig. 4.2 shows the effect of OH on the heat capacity of SiO_2: a sample containing 1200 ppm of OH has a heat capacity larger by about 30% than a sample containing less than 1.5 ppm.

4.2 Metallic Glasses

The existence of free electrons in amorphous metals makes it difficult to deduce the presence of tunnelling states from the thermal properties. By estimating the electronic contribution to the thermal conductivity, using the Weideman-Franz ratio and the measured electrical conductivity, the phonon contribution to κ can be shown to resemble that of amorphous insulators. However, the most direct thermal evidence comes from measurements on amorphous superconductors, as shown in Fig. 4.3 for Zirconium-Palladium. Below the transition temperature T_c of 2.5 K the electronic contribution to the heat capacity vanishes exponentially, and the resulting linear term at very low temperatures can be identified with tunnelling states. Below T_c heat is carried only by phonons, and as shown in Fig. 4.4 the temperature dependence of κ is very similar to that found in vitreous silica. The magnitude of κ in $Zr_{70}Pd_{30}$ is smaller, but if the results are used to calculate $\bar{n}\gamma^2$ using eqs 1.1 and 2.14, a value of approximately 5×10^{46} J m^{-3} is found, half that of vitreous silica or NiP but typical of other amorphous metals.

As in insulating glasses, acoustic measurements provide the most direct evidence for two-level systems in metallic glasses. The most straightforward experiment, in which effects of saturation can be ignored, is the measurement of the temperature variation of the acoustic velocity. Results in NiP are shown in Fig. 4.5. A logarithmic variation of velocity with temperature is observed, as in silica, although the slope is smaller by an order of magnitude, and is significantly different for longitudinal and transverse waves. A value of $\bar{n}\gamma^2$ of 3×10^{46} J m^{-3} can be calculated from either slope (unlike silica where $\bar{n}\gamma^2$ is larger by a factor of two for longitudinal waves). This should be compared with the value of about 15×10^{46} J m^{-3} estimated from the phonon contribution to κ. It is clear that unlike the insulating glasses, where in general the values of $n\gamma^2$ derived from thermal and acoustic measurements are in good agreement, there is a major discrepancy in amorphous metals.

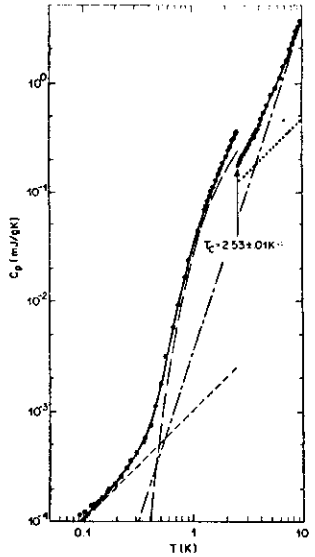

4.3 Heat capacity of superconducting amorphous $Zr_{0.7}Pd_{0.3}$ (J.E. Graebner, B. Golding, R.J. Schutz, F.S.L. Hsu and H.S. Chen, Phys. Rev. Lett., 39, 1480, 1977).

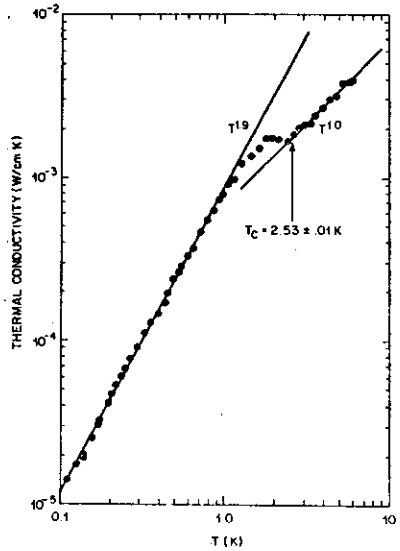

4.4 Thermal conductivity of superconducting amorphous $Zr_{0.7}Pd_{0.3}$ (J.E. Graebner, B. Golding, R.J. Schutz, F.S.L. Hsu and H.S. Chen, Phys. Rev. Lett., 39, 1480, 1977).

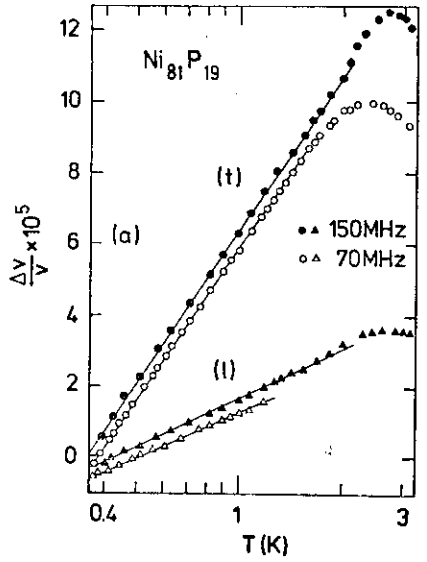

4.5 Variation of acoustic velocity in amorphous $Ni_{81}P_{19}$ (H. v Lohneysen, Phys. Rep., 79, 161, 1981).

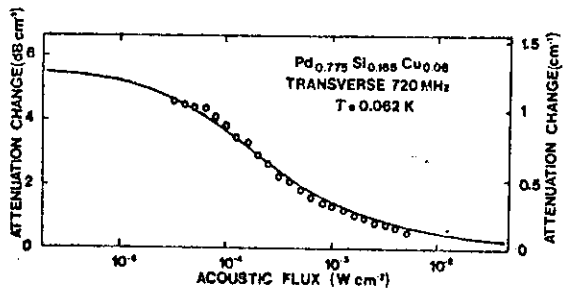

4.6 Attenuation as a function of intensity in the amorphous alloy Pd-Si-Cu (P. Doussineau, P. Legros, A. Levelut and A. Robin, J. Physique, 39L, 265, 1978).

Further experimental evidence emphasizes that the tunnelling-state theory cannot be applied directly to metals. Two-pulse saturation experiments as described in section 3, have been completely unsuccessful even at temperatures of 10 mK. At this temperature T_1 in silica is 200 μs (at a frequency of 1 GHz) but the failure of attempts to measure T_1 in PdSiCu imply that it is less than 25 ns under these conditions. If T_1 were governed by one phonon processes in this glassy metal, the value of the coupling constant γ would need to be at least an order of magnitude larger than in silica. This is clearly inconsistent with the thermal results.

This rapid relaxation is a result of direct interaction of the tunnelling states with the electrons. Electrons are inelastically scattered from tunnelling systems in a process which is formally equivalent to nuclear spin relaxation in metals. The magnitude of T_1 can be derived from the Fermi expression for transition probabilities, so that the probability per unit time of an electron exciting a tunnelling state is

$$\omega_{ij} = \frac{2\pi}{h} K^2 g(\epsilon_F)$$

where K is the electron-tunnelling state matrix element and $g(\epsilon_F)$ is the density of electronic states evaluated at the Fermi level. If the energy splitting E of the tunnelling state is less than k_BT than the number of electrons capable of inducing the transition is $g(\epsilon_F)k_BT$, and the time between transitions $1/T_1$ is given by

$$\frac{1}{T_1} \approx \frac{2\pi}{\hbar} \{Kg(\epsilon_F)\}^2 k_BT \quad . \qquad 4.1$$

For $E > k_BT$ the kT factor is replaced by one obtained from integrating over the Fermi factors to give

$$\frac{1}{T_1} = \frac{2\pi}{\hbar} \{Kg(\epsilon_F)\}^2 E \coth \frac{E}{2k_BT} \quad . \qquad 4.2$$

Estimating K, the difference in potential seen by the electrons in the two configurations of the tunnelling state, as 1eV and taking $g(\epsilon_F)$ as 0.1 $(eV)^{-1}$ per atom gives $T_1 \sim 10$ ns at 10 mK, consistent with experiment.

This short relaxation time not only explains the absence of phonon echoes but also implies that the acoustic power needed to saturate the tunnelling states will be much higher than in vitreous silica. The interaction with electrons provides another channel through which equilibrium of the tunnelling states can be maintained, and the saturating acoustic power should be larger by the ratio of electron and phonon scattering rates. Experimental results, verifying this prediction, are shown in Fig. 4.6.

The magnitude of T_1 has an indirect effect on κ. In addition to the resonance scattering of phonons by tunnelling states, it is also possible to identify a relaxation contribution. The strain field of a non-resonant phonon of frequency ω perturbs the equilibrium of a tunnelling state through the coupling γ. The tunnelling state returns to equilibrium with a relaxation time T_1 so that at low frequencies $\omega T_1 << 1$ equilibrium is always maintained. At high frequencies $\omega T_1 >> 1$ the tunnelling state does not have time to respond to the strain field, but for $\omega T_1 \sim 1$ the response will lag behind the strain. This phase difference gives rise to a relaxation loss which can be formally described by means of the Debye equations, written in slightly simplified form and using τ in place of T_1.

$$\ell_{rel}^{-1} = \frac{\bar{n}\gamma^3}{\rho v^3 k_BT} \int_0^\infty \operatorname{sech}^2 \frac{E}{2k_BT} \int_{\tau_{min}}^\infty \frac{\omega^2\tau}{1+\omega^2\tau^2} g(\tau) d\tau \quad . \qquad 4.3$$

$$\frac{\Delta v}{v} = \frac{\bar{n}\gamma^2}{2\rho v^2 k_BT} \int_0^\infty \operatorname{sech}^2 \frac{E}{2k_BT} dE \int_{\tau_{min}}^\infty \frac{g(\tau)}{1+\omega^2\tau^2} d\tau \quad . \qquad 4.4$$

Physically the first factor in eq. 4.3 is the contribution from a simple elastic dipole, the first integral excludes all states which have $E > k_BT$ and so remain in thermal equilibrium, while the second integral describes the relaxation. In general the first integral gives a factor k_BT, and the dominant factor in $g(\tau)$ is $1/\tau$, following the argument leading to eq. 1.15. Equations 4.3 and 4.4 become, in this simplified form

$$\ell_{rel}^{-1} = A \int_{\tau_{min}}^\infty \frac{\omega^2}{1+\omega^2\tau^2} d\tau = A\omega\left(\frac{\pi}{2} - \tan^{-1} \omega \tau_{min}\right) \quad . \qquad 4.5$$

$$\frac{\Delta v}{v} = B \int_{\tau_{min}}^\infty \frac{1}{(1+\omega^2\tau^2)\tau} d\tau = B \ln(\omega^2\tau^2_{min}/1+\omega^2\tau^2_{min}) \quad . \qquad 4.6$$

If $\omega\tau_{min} > 1$

$$\ell^{-1} = A/\tau_{min} \quad , \quad \Delta v/v = -B/\omega^2\tau^2_{min} \qquad 4.7$$

and if $\omega\tau_{min} < 1$

$$\ell^{-1} = A\omega \quad , \quad \Delta v/v = B \ln(\omega^2\tau^2_{min}) \quad . \qquad 4.8$$

In insulating glasses $\tau_{min} \approx aT^{-3}$ where a is 10^{-8} sK^3 so that for typical

acoustic frequencies $\omega\tau_{min} = 1$ at about 2 K. In this temperature region the rapid variation $\Delta v/v = -BT^6/a^2\omega^2$ gives rise to the 'turnover' of the velocity shown in Fig. 2.5, and $\ell^{-1} = AT^3/a$ to the upturn in attenuation shown in Fig. 1.5 at higher temperatures.

In metallic glasses the relaxation time τ (or T_1) is much shorter, with $\tau_{min} \simeq bT^{-1}$ where $b \simeq 10^{-10}$ sK in the low temperature regime where electronic processes dominate. Phonon scattering becomes important at a temperature T_o given by $bT_o^{-1} = aT_o^{-3}$, or about 10 K. At an acoustic frequency of 1 GHz $\omega\tau_{min} \sim 1$ at approximately 100 mK. This means that the logarithmic slope measured in an acoustic experiment contains contributions from both resonance and relaxation terms, as does the measured attenuation. Since the two contributions are of different sign in the velocity, but add in the attenuation, the values of coupling constant deduced from the velocity variation are significantly smaller than those deduced from the acoustic attenuation or thermal conductivity. Detailed calculation of the relaxation contribution have been made in PdSiDu, and agree well with experiment.

The effects of electrons in determining T_1 are dramatically confirmed by acoustic measurements in amorphous superconductors. Attenuation as a function of temperature is shown in Fig. 4.7 for $Pd_{30}Zr_{70}$. These results can be explained by noting that from eq. 4.8 the attenuation ℓ^{-1} is not sensitive to the details of the relaxation process if $\omega\tau << 1$, but depends only on frequency. In this limit, satisfied above T_c in $Pb_{30}Zr_{70}$, the attenuation is constant even though the phonon and electron contributions to the tunnelling state lifetimes are varying as T^{-3} and T^{-1} respectively. Below T_c the number of effective electrons drops as a result of the superconducting energy gap, but in the amorphous superconductor, where the direct electron-phonon interaction does not give significant attenuation, this is not immediately effective. Only when T_1 has increased to such an extent that $\omega T_1 > 1$ does the attenuation drop following eq. 4.7. This will occur at approximately $T_c/2$, where the electron contribution to T_1 becomes negligable in comparision to the phonon. Below $T_c/2$ the attenuation will decrease as T^3, characteristic of phonon processes.

The most complete microscopic description of a possible intrinsic tunnelling state comes from results on Nb/Zr alloys. Although crystalline, this material is disordered in the sense that it contains small amounts of the ω phase in a matrix of the β phase. In a 20% Nb sample isolated regions of ω phase, about 5 Å in diameter, are formed at a concentration of about 10^{25} m^{-3}. Results for the heat capacity and κ show that glassy behaviour can be obtained in this disordered crystal, and furthermore that this behaviour can occur where the disorder is localised to very small regions separated by about 100 Å.

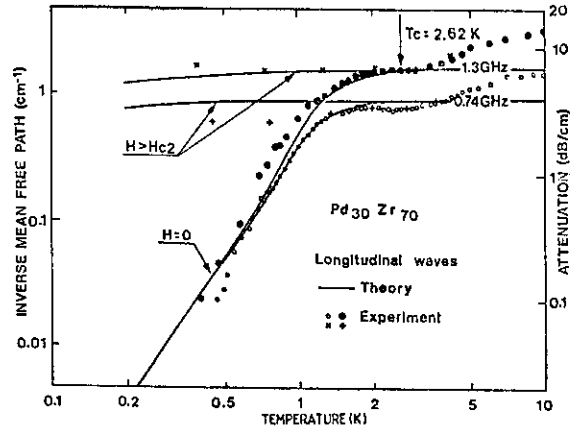

4.7 Attenuation of sound in superconducting amorphous $Pd_{30}Zr_{70}$ (W. Arnold, P. Doussineau, Ch. Frénois and A. Levelut, J. de Physique Lett., 42, L289, 1981).

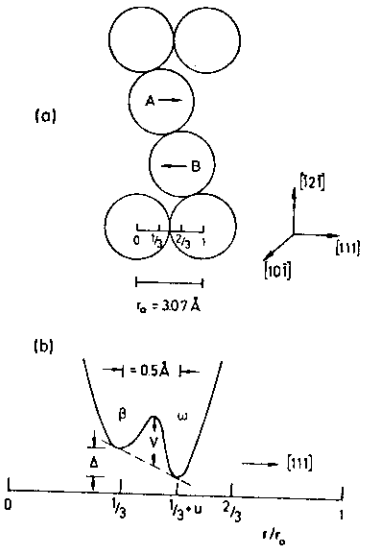

4.8 Schematic representation of the β-ω phase transition in Zb/Zr. (L.F. Lou, Solid State Com., 19, 335, 1976.)

The microscopic picture of the states responsible for the additional heat capacity and the T^2 variation of κ is reasonably well established in the Nb/Zr alloy. The β-ω transformation occurs by moving two atoms simultaneously through a distance of about 0.5 Å as shown in Fig. 4.8. The potential for each atom can be described by a double potential well, and it appears on the basis of electron microscopy, inelastic neutron and Mössbauer measurements, that a large range of potential barriers V must exist in the solid. Such a microscopic state could easily exist in the glassy metals, and is exactly of the form suggested by the tunnelling model.

4.3 OH in Vitreous Silica

The effect of hydroxyl, OH, on the low temperature properties of vitreous silica has been investigated in a wide range of experiments comparing commercial 'water free' and 'wet' samples. An example is given in Fig. 4.2. The various experiments can be related and linked to form a consistent picture of one particular impurity tunnelling state.

The chemistry of OH in silica has been extensively studied in connection with the growth of 'wet' oxide films on silicon and with the optical absorption arising from OH stretching vibrations, of particular importance in applications of optical fibres. The general conclusion of these studies is that the chemical reaction $Si\text{-}O\text{-}Si + H_2O \rightarrow 2SiOH$ gives rise to OH groups chemically bonded to the silica network. The intensity of the fundamental OH stretching vibration is proportional to OH concentration, but the width of the absorption line is constant, indicating that in general interactions between OH groups can be neglected. However, the absorption line is broad ($\Delta\nu/\nu \sim 5\%$) indicating that interactions between OH and the silica host *are* important. Each OH group can therefore be treated independently of the others, moving in a potential which varies considerably from site to site.

In organic compounds an OH group bonded to a carbon atom can rotate in a twofold (phenols) or threefold (tertiary alcohols) symmetric potential, although the ideal symmetry is of course modified in the solid state by intermolecular interactions. A similar picture can be used for OH in silica with the choice of 'symmetry' left to experiment: because the interactions between OH and its surroundings are large, there is no *a priori* reason for preferring the threefold potential given by the tetrahedral coordination of the Si atom.

Figure 4.9 shows that the effect of 1200 ppm OH on the dielectric loss of vitreous silica is to produce a broad low temperature relaxation peak. The physical interpretation of relaxation losses is as described in the last section, but in this case the information is sufficiently complete to

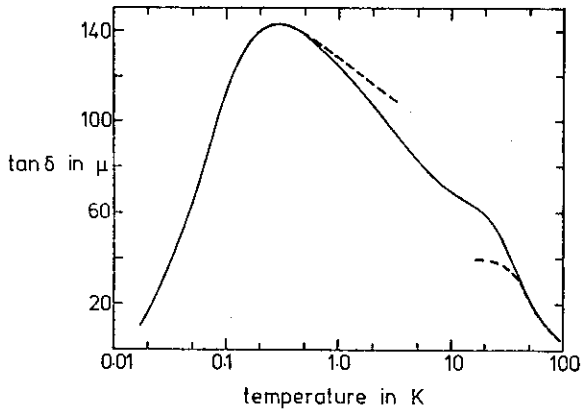

4.9 The contribution of 1200 ppm OH to the dielectric loss of vitreous silica. (W.A. Phillips, Phil. Mag., B43, 747, 1981.)

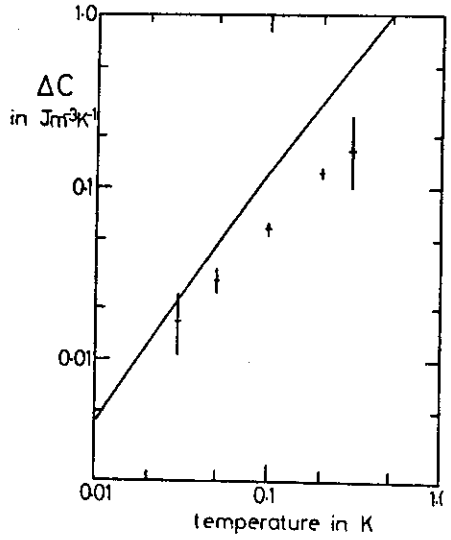

4.10 The contribution of 1200 ppm OH to the heat capacity of vitreous silica. The solid line is calculated. (W.A. Phillips, Phil. Mag., B43, 747, 1981.)

allow the distribution function $g(\tau)$ to be derived. At high temperatures a classical theory can be used to deduce the distribution of energy barriers from $g(\tau)$, and this in turn can be used to derive $g(\Delta_o)$. It turns out that the real $g(\Delta_o)$ differs from eq. 1.15 by having fewer small values of Δ_o, and corresponds to the proton 'rotating' in an approximately two-fold symmetric potential.

Knowing $g(\Delta_o)$ together with the dipole moment p_o of eq. 2.1 allows the temperature variation of the velocity of light, shown in Fig. 2.6, to be calculated. The departure of $g(\Delta_o)$ from $1/\Delta_o$ means that the logarithmic slope, given by eq. 2.21, depends on measuring frequency: the available data can be well fitted by the calculation. In addition the density of states can be calculated, following eqs 2.15 to 2.17, and this leads to a calculated value of the heat capacity which agrees with the difference between the two sets of data shown in Fig. 4.2. This is shown in Fig. 4.10. Finally, the idea of OH as a discrete tunnelling state is consistent with photon echo experiments, although precise numerical calculations are difficult.

This detailed analysis of one kind of impurity is useful in that it shows how impurities can contribute to the low temperature properties but it is equally clear, from Figs 4.2 and 3.2, that other, possibly intrinsic, two-level systems are present. The nature of these intrinsic states is unknown, although a number of possibilities have been proposed, and will be discussed in the next section.

4.4 The Structural Origin Of Tunnelling States

Sections 1, 2 and 3 described the theory of the tunnelling model and how it accounts for a variety of experiments on amorphous solids at low temperatures. This section attempts to identify the possible atomic scale origins of the tunnelling states in simple covalently bonded inorganic glasses such as vitreous silica, elemental amorphous semiconductors Se, As, P, Ge and Si and chalcogenide glasses such as $Ge_x Se_{1-x}$, As_2S_3 and As_2Se_3. The structure of all these materials seems to be best described by the continuous random network (CRN) model, and models for the origin of double-well potentials usually involve atomic motion without bond-breaking. The double-well is often associated with a two-fold coordinated atom, e.g. oxygen in silica, or with similar displacements to those observed in transitions between two crystalline forms. There is a strong case for the existence of double-well potentials from the ultrasonic attenuation peak at around 50 K and from the onset of large atomic movement near the glass transition T_g.

In a defect-free CRN, each atom forms the same number of covalent bonds with its neighbours (often 8-N, where N is the group in the periodic table). If more than one type of atom is present, chemical ordering is possible. X-ray diffraction and other structural studies demonstrate that long range order is absent, but short range order is often similar to that of the corresponding crystal. The radial distribution (r.d.f.) gives the coordination number and demonstrates that the bond length is fixed, variations arising chiefly from thermal vibrations. On the other hand, the bond angle generally has a spread of 10 - 20° about a mean value. The r.d.f. does show broad peaks at larger distances, but often features present in the crystalline form are completely absent. In the CRN model, this is achieved by allowing the dihedral angle (defining rotation about a bond) to take a continuous spectrum of values.

The tunnelling model attributes the low temperature behaviour of glasses to the existence of double-well potentials. From their energy possible combinations of the parameters V, d and m (barrier height, width and mass of tunnelling species) can be deduced. For example, an oxygen atom tunnelling 0.1 nm through a potential barrier of height 8×10^{-22} J (5×10^{-3} eV or 60 K) gives a state of energy equivalent to 1 K, assuming that the vibration frequency Ω is given by the Debye frequency (θ_D = 495 K in vitreous silica). A state of energy 0.05 K requires a barrier of twice the height.

Some of the proposed origins of the double-well potentials were originally advanced in connection with the ultrasonic attenuation peak at 50 K in vitreous silica. Anderson and Bömmel proposed that the relaxing unit was an oxygen atom "flipping" between two equilibrium positions transverse to the Si - O - Si bond. This change does not preserve the O - Si - O bond angles at the two silicon atoms involved, and so the true equilibrium configuration must involve a local rearrangement of the network to minimise the strain energy of the bonds. This model is attractive for the majority of amorphous solids, which contain two-fold coordinated atoms. However, the three-fold coordinated materials a-As and a-P both show a similar peak in the ultrasonic attenuation and a small excess low temperature heat capacity although the structure of these two materials is much less perfect than that of most bulk glasses. Low temperature heat capacity experiments give no clear evidence for a linear term in amorphous Ge and surface wave attenuation measurements are consistent with the absence of double-well potentials: in a-Si the logarithmic sound velocity variation indicates that $\bar{n}\gamma^2$ is at least a factor of 12 lower than in an SiO_2 film.

Estimates of the total number of double well potentials from the 50 K ultrasonic attenuation peak lead to typical values of 1 per 100 atoms in SiO_2, a-As, a-P and many other materials. The required potential barrier in vitreous silica is obtained from an initial Si ~ O - Si angle of 174°. The experimental r.d.f. shows around 1% of the Si - O - Si bond angles in this range, in good agreement. In three-fold coordinated materials, if the model applies, the pyramidal unit must be rather flatter than usual, with the bond angles larger than their usual values, probably close to 120°.

Vukcevich developed a model for vitreous silica which also invokes a potential function which possesses two minima separated by a barrier. Whole SiO_4 tetrahedra can assume one of two equilibrium positions, the fraction in each varying with temperature. The model seems difficult to reconcile with the random network model, as the four Si atoms at the centres of the neighbouring tetrahedra need to be situated so that a rotation of the central tetrahedron changes all four Si - O - Si bond angles in the same sense, but is based on the structural changes seen in the α-β displacive transition in quartz at 545°C.

Mon and Ashcroft gave essentially the same argument for the origin of double-well potentials. They also connected the occurrence of the amorphous state and crystal polymorphism with the existence of low temperature thermal anomalies.

A useful step would be to search CRN models by computer for double-well potentials. Smith used a four-fold coordinated model representing a-Ge and a-Si. One atom at a time was moved and the energy calculated, but the surrounding network was not allowed to relax. Many large barriers and large asymmetries were found (4 per atom) but the numbers at low Δ_0 and Δ were of the right order of magnitude to give a typical excess specific heat. Similar, but more realistic calculations would give a very useful guide to the microscopic nature of the tunnelling systems.

A variety of electrical and optical measurements on amorphous semiconductors suggests a broad division into two types of material. Both possess mobility edges separating extended from localised states in the valence and conduction bands, and the Fermi level is pinned at around mid-gap, i.e. it does not shift with temperature or on the addition of impurities. This suggests a density of localised defect states in the band gap. The first group of materials includes a-Ge and a-Si prepared in the absence of hydrogen and oxygen and at low temperatures shows an e.s.r. signal in the dark and d.c. conductivity proportional to $\exp(-T/T_o)^{1/4}$ where T_o is a constant. This law can be derived for variable range hopping of electrons between localised states at E_F. Both observations suggest that defect states at the Fermi level are singly occupied at absolute zero.

The second group encompasses the chalcogenide glasses; most work has been performed on As_2S_3, As_2Se_3 and Se. Variable range hopping and a dark e.s.r. signal are not observed. There are, therefore, no single electrons at E_F to give a linear heat capacity in chalcogenide (and oxide) glasses. However, an e.s.r. signal (and optical absorption at mid-gap) can be induced by irradiation with slightly sub-band-gap light, and removed by annealing above typically 100 K or by irradiation with infra-red radiation at around half the band gap. These materials also show photoluminescence at about half the band gap when irradiated with band-gap light.

These and other experimental results were brought together and explained using a simple model by Street and Mott based on a spin pairing idea of Anderson. The model assumes the presence of defects in amorphous materials above their T_g, in much the same way as a thermal equilibrium concentration of vacancies and other defects exists in crystals. These defects are "frozen in" during quenching or deposition. The simplest defect imaginable is a "dangling bond" where the coordination is not satisfied at one atom in an otherwise perfect random network. Such a structure can be constructed with a variety of local environments and the dangling bond orbital can be unoccupied (D^+), single occupied (D^o) or doubly occupied (D^-). This notation of Street and Mott is used to specify the charge state of the defect. In a-Si and a-Ge, the centres in the gap are singly occupied (D^o) giving rise to the e.s.r. signal. In chalcogenides, however, Street and Mott proposed that equal numbers of D^+ and D^- states are energetically favoured to D^o, accounting for the absence of unpaired electrons. The correlation energy, usually positive due to electron-electron repulsion favouring singly occupied levels, is effectively negative due to lattice relaxation around the D^+ defect. The stability of the charged defect states is confirmed by theoretical studies and chemical bond arguments which can also predict the coordination and position in the band-gap. Other support for the existence of under-coordinated and over-coordinated atoms has come from the observation of small sharp features in the infra-red and Raman spectra of several amorphous solids, notably silica and a-As.

One modification of this model is to suppose that oppositely charged defects do not occur at random but form preferentially in close proximity, gaining electrostatic energy and producing a neutral centre (the "intimate valence alternation pair" or IVAP of Kastner). In a model for the a.c. conductivity of chalcogenide glasses based on thermally activated hopping of electron pairs from D^- to D^+, Elliott found that pairs of defects only 0.5 nm apart dominate, in contrast to the 10 nm mean separation. As discussed below, it is likely that if electron tunnelling between charged

defects is responsible for the formation of the two-level systems, the defects need to be closely spaced.

At least one experiment on As_2S_3 reveals interesting correlations between charged defects and two-level systems. This used electric echoes to probe tunnelling states in As_2S_3. After irradiation with band gap light (2.41 eV) the echo signal is reduced but can be progressively restored by annealing at increasingly higher temperatures or by irradiation with mid-gap (1 - 2 eV) radiation. The magnitude of the echo signal therefore corresponds to the population of the D^+ (or D^-) centre; excitation to D^o reduces the echo signal.

However, the link between charged defects and two-level systems is uncertain. Single electron hopping, either thermally activated or by phonon assisted tunnelling, is excluded at low temperature owing to the large energy required (about half the band-gap) to transfer the electron to another site. Hopping of two electrons together is therefore the only possibility, but the rate for phonon assisted tunnelling is vanishingly small unless the separation between sites is of order 0.1 nm, corresponding to the IVAP. Structural relaxation around the initial and final positions of the electron pair therefore involves esssentially the same atoms, and the transition can be equally well described in terms of a potential barrier to atomic motion. The transition may involve interchange of D^+ and D^- centres as in the Elliott model, or the other bond rearrangements. Alternatively, the coordination of each atom may remain fixed and the charged defect (presumably an under-coordinated atom in this case) merely makes the lattice locally less rigid allowing a double potential well to form.

Whilst the electric echo experiments of Golding in As_2S_3 clearly demonstrate a link between the charged defect centres and two-level systems, a structural model based on atomic tunnelling still appears preferable. The existence of potential barriers of the required height and width seems very plausible based on current views of the glass transition: tunnelling states are a necessary consequence of their existence. Two-level systems also occur in polymers and amorphous metals: the only common feature is structural disorder. It is attractive to believe that this results generally in double potential wells.